CHARACTERIZATION OF THE HUMAN ALPHA RHYTHM BY ENVELOPE ANALYSIS

Thesis submitted to the University of Chile in partial compliance with the requirements to qualify for the Master's Degree in Biological Sciences

Faculty of Sciences

by

Víctor Manuel Hidalgo Ibarra

July 2021

Thesis Director: Dr. Juan Carlos Letelier Parga

Thesis Co-Director: Dr. Jorge Mpodozis Marin

FACULTAD DE CIENCIAS

UNIVERSIDAD DE CHILE

INFORME DE APROBACION

TESIS DE MAGÍSTER

Se informa a la Escuela de Postgrado de la Facultad de Ciencias que la Tesis de Magíster presentada por el candidato:

Víctor Manuel Hidalgo Ibarra

Ha sido aprobada por la comisión de Evaluación de la Tesis como requisito para optar al grado de Magíster en Ciencias Biológicas con mención Biología Molecular, Celular y Neurociencias, en el examen de Defensa Privada de Tesis rendido el día 10 de Septiembre de 2021.

Director de Tesis

Dr. Juan Carlos Letelier Parga .....

Co-Director de Tesis

Dr. Jorge Mpodozis Marin .....

Comisión de Evaluación de la Tesis

Dr. Julio Alcayaga Urbina .....

Dr. Osvaldo Álvarez Araya .....

DEDICATION

Quisiera dedicar este trabajo a la mamá Carolina Ibarra, a quien debo el beneficio de la ciencia. En efecto, más allá del acto puramente mayéutico, es Carolina quien vio en mí la necesidad de seguir un camino ilustrado. Es Carolina quien me integró al Liceo José Victorino Lastarria y me inculcó una disciplina olímpica, y quien luego me instó a continuar mi educación en la Universidad de Chile. Aún más importante, el implacable afecto por el otro de Carolina y su sencillez ha guiado mi actuar desde el momento que la memoria surgió en mí, y cual armadura me ha protegido de los proyectos personales disfrazados de generosidad y de la inteligencia degenerada en despotismo; en buenas cuentas, de la indecencia presentada como su opuesto. En la búsqueda del arte de ser humano, me he encontrado con que muchos pregonan pero son contados los que gozan de la rectitud de Carolina. ¡Qué suerte la mía! Así mismo, también dedico este trabajo al papá Juan Manuel y al hermano Maximiliano, los quiero.

BIOGRAPHY

Nací en Santiago y realicé mis estudios básicos y medios en el Liceo José Victorino Lastarria, para luego cursar el programa de biología en la Facultad de Ciencias de la Universidad de Chile. Posteriormente, ingresé al programa de Magíster en Ciencias Biológicas en la misma casa de estudios, donde me enfoqué en la electroencefalografía y su análisis digital, realizando mi trabajo de investigación en el Laboratorio de Neurobiología y Biología del Conocer.

ACKNOWLEDGEMENTS

Quisiera agradecer a tantos tutores que han tenido conmigo la delicadeza de contestar el teléfono a toda hora. Aún recuerdo cuando en mi primer día de universidad me dirigí directamente a conocer el laboratorio de Biología del Conocer, junto a mi amigo Rodrigo Toledo. Al llegar a la puerta de vidrio, me encontré con el Dr. Juan Carlos Letelier y el Dr. Jorge Mpodozis frente a frente y recibí la bienvenida más heterodoxa que uno pudiese imaginar. Agradezco a ellos y también al Dr. Máximo Fernandez por estar en "el Rayo" para sus estudiantes. También a agradezco a Rodrigo Toledo por siempre decirme lo que piensa. Además debo agradecer a Marjorie Luengo, Angélica Bachelet, Jorge Alarcón y Lama Karma Chötso por guiarme en el arte de ser humano.

CONTENTS

LIST OF TABLES

LIST OF FIGURES

LIST OF ABBREVIATIONS

AN-iEEG	Atlas of the Normal Intracranial Electroencephalogram
CVE	Coefficient of Variation of the Envelope
DFT	Discrete Fourier Transform
EC	Eyes-closed
EEG	Electroencephalography
EnvEEG	EEG Envelope Analysis
EnviEEG	IEEG Envelope Analysis
EnvSpace	Envelope Characterization Space
EO	Eyes-open
ERD	Event-related Desynchronization
ERS	Event-related Synchronization
FIR	Finite Impulse Response
FT	Fourier Transform
HT	Hilbert Transform
IDFT	Inverse Discrete Fourier Transform
iEEG	Intracranial Electroencephalography

IIR	Infinite Impulse Response
LEMON	Leipzig Study For Mind-body-emotion Interactions
ME	Mean of the Envelope
MMS model	Matthews–Mirollo–Strogatz Model
PDF	Probability Density Function
rs-EEG	Resting-state Electroencephalography
rs-iEEG	Resting-state Intracranial Electroencephalography
WCO	Weakly Coupled Oscillators
WGN	White Gaussian Noise

RESUMEN

El ritmo alfa es un patrón de actividad eléctrica revelado por registros de electroencefalografía (EEG), el cual fue primeramente descrito por el Dr. Berger en individuos despiertos con los ojos cerrados, desapareciendo cuando los sujetos abren los ojos. La caracterización habitual de este fenómeno muestra actividad específica en el espacio y tiempo, distinguida como aumento de la potencia del espectro en la banda alfa (8-13 Hz) de señales obtenidas desde la región occipital del cuero cabelludo. Sin embargo, esta caracterización no permite realizar afirmación ninguna acerca de la dinámica de las poblaciones neuronales participantes. El análisis de la envolvente ofrece una herramienta para evaluar dicho comportamiento a partir de señales de EEG. En particular, este metodo se basa en el hecho de que el coeficiente de variación de la envolvente (CVE) de un proceso Gaussiano es una constante de la naturaleza igual a $\sqrt{(4-\pi)/\pi} \approx 0.523$. Registros asincrónicos muestran un CVE cercano a esta constante, mientras que procesos sincronicos son detectados como desviaciones significatives de este valor de referencia. El análisis demostró que el ritmo alfa se comporta como un proceso Gaussiano y sincrónico debido a variabilidad intra e intersujeto. En cambio, la observación inicial de Berger respecto del cambio de energía entre condiciones experimentales se mantuvo independientemente de los valores de CVE involucrados. En luz de estos resultados, las implicancias para los campos del EEG y el análisis de señales son discutidas.

ABSTRACT

The alpha rhythm is an electrical activity pattern revealed by electroencephalography (EEG) recordings, which was first described by Dr. Berger in awake subjects with their eyes closed, disappearing when subjects open their eyes. The usual characterization of this phenomenon shows specific temporal and spatial activity, distinguished as an increase of the spectral power in the alpha band (8-13[Hz]) in signals obtained from the occipital region of the scalp. Nevertheless, this characterization allows making no assertion about the dynamics of the participating neural populations. The envelope analysis offers a tool to evaluate such behavior from EEG signals. In particular, this method is based on the fact that the coefficient of variation of the envelope (CVE) of a Gaussian process is a universal constant equal to $\sqrt{(4-\pi)/\pi} \approx 0.523$. Asynchronous recordings show a CVE close to this constant, while synchronous processes are detected as significant deviations from this reference value. The analysis demonstrated that the alpha rhythm behaves as a Gaussian and a synchronous process due to intra- and inter-subject variability. On the other hand, Berger's initial observation regarding the energy change between experimental conditions held regardless of the CVE values involved. In light of these results, the implications for the EEG and signal analysis fields are discussed.

INTRODUCTION

The *human alpha rhythm* was the first phenomenon to be described in the field of *electroencephalography* (EEG) (Berger, 1929), and thus it resides at the very foundation of the discipline. While the alpha rhythm is at the heart of basic and clinical EEG research, its origin is still a matter of debate. Interestingly, in spite of massive research efforts encompassing many decades, the temporal dynamics of the underlying neural populations contributing to this rhythm, and to EEG in general, has not been clearly identified and characterized (Cohen, 2017). Therefore, a better understanding of the temporal dynamics of the alpha rhythm generator is of significant importance for the field of EEG research. Here, I will advance in this question by expanding an intuition of Díaz et al. (2007) that uses the *coefficient of variation of the envelope* (CVE) to characterize amplitude modulation patterns, thus discriminating between Gaussian and synchronous dynamics. My contribution will be centered on using the envelope analysis to test this viewpoint — an analysis that crucially depends on the concept of a signal envelope (a concept not usually used in current neuroscience).

1.1 Electroencephalography

EEG is the study of the brain's electrical fields by means of electrodes placed on the scalp surface (Niedermeyer and Lopes da Silva, 2005). As a research tool, EEG offers information about brain function at a macroscopic scale with high temporal resolution (1 ms) and low cost implementation, characteristics that make it the preferred method in applications such as medical imaging, human-computer interaction, seizure detection, among others (ibid.). Thus, even though the origin of the discipline is traced back to the 1920s, EEG is today an active field of research in the advancement of the understanding of both normal and abnormal brain dynamics (Cohen, 2017).

1.1.1 Origin and Development of EEG

Human EEG has its origin in the works of Dr. Hans Berger (1873-1941), a German psychiatrist working at University of Jena before and after World War I (Gloor, 1969). While the study of animal brain electrical activity had already been developed — the first report was published by Lord Richard Caton (1842-1926) in 1875 (Caton, 1875) — Berger studied for the first time signals recorded from the scalp of human subjects using a D'Arsonval galvanometer. In "Über das elektrenkephalogramm des menschen" (About the human electroencephalogram) (Berger, 1929), he reported two types of electrical activity, one of high amplitude and low frequency and other of low amplitude and high frequency. The first signal was present when the subjects

kept their eyes closed and the second one when they had their eyes open. Dr. Berger dubbed these two rhythms alpha and beta, respectively (Buzsáki, 2006). Subsequently, he released many more reports based on data from patients under different conditions, such as epilepsy, psychosis, and anesthesia (reviewed by Gloor, 1969).

Nevertheless, history tells us that Mr. Berger's work was not deemed trustworthy by some of his colleagues (Niedermeyer, 2005a). First of all, he trained as a clinician, and physiologists looked down upon his capacity to conduct experiments properly (Gloor, 1969). Additionally, his work was published in German, a trait that rendered it difficult to access (ibid.). Perhaps more egregious was Berger's metaphysics. His real intention behind the study of brain electricity was to explore the mind-body connection and to find what he called psychic energy; an enterprise preposterous for many (Millett, 2001).

In this context, the work of Lord Edgar Douglas Adrian (1889-1977) was pivotal for the acceptance of Berger's results. Adrian, a quintessential Cambridge *Don*, was one of the most eminent electrophysiologists of his time. In fact, he was awarded in 1932, together with Sir Charles Sherrington (1857-1952), the Nobel Prize in Physiology or Medicine "for their discoveries regarding the functions of neurons", specially the famous *all or none law* regarding neuronal firing (Grant, 2006). Adrian repeated Berger's experiments making several important contributions to the field. First, he confirmed that waves of around 10 [Hz] can be recorded from human subjects under the conditions specified by Berger (Adrian and Matthews, 1934a). This replication

brought about the acceptance of Berger's claims by the scientific community (Lopes da Silva, 1991). Second, while Berger considered the alpha rhythm to emerge from the entire cortex, Adrian provided evidence to locate the origin at the occipital cortex (Adrian and Matthews, 1934a) — a point confirmed by a subsequent report (Adrian and Yamagiwa, 1935). Furthermore, Adrian interpreted that the emergence of the human alpha rhythm is triggered by the synchronized activity of the underlying neural population, and conversely that its disappearance happens when this population enters into a desynchronized regime (Adrian and Matthews, 1934a; Hodgkin, 1979). More importantly, this claim became the fundamental interpretation for EEG phenomena (Pfurtscheller and Lopes da Silva, 1999; Rao and Edwards, 2008).

In the following years, many European and American EEG groups quickly developed, and finally electroencephalography emerged as a well-defined field of study (Niedermeyer, 2005a). In 1935 the first 3-channel EEG machine was built at Harvard Medical School (Grass, 1984), and in 1938 the Fourier transform of EEG recordings was obtained (Grass and Gibbs, 1938). Several applications for EEG also emerged, while some researchers delineated the electrical activity during epileptic seizures (Gibbs et al., 1935), others characterized the EEG during sleep (Loomis et al., 1935). By the 50s, electroencephalography was already a widespread practice, both as basic and clinical science (Niedermeyer, 2005a).

1.1.2 The EEG Signal

The origin of the EEG signal resides in the postsynaptic currents of populations of pyramidal neurons in the neocortex (Lopes da Silva and van Rotterdam, 2005). Evidence for EEG cortical origin was provided early by Adrian. He recorded simultaneously from electrodes placed directly on the cortical surface and from subcortical electrodes. He found that the EEG signal was present when recorded from the cortical surface and was not measured in white matter (Adrian and Matthews, 1934b). The postsynaptic and pyramidal origin is substantiated by pharmacological and electrophysiological evidence (Avitan et al., 2009). For instance, Purpura and Grundfest (1956) reported that the use of d-tubocurarine in cat abolishes evoked dendritic activity in cortical cells, with the concomitant disappearance of cortical surface signals. In the same model, Jasper and Stefanis (1965) studied the pyramidal tract and found that the cortical surface signals were not affected by individual pyramidal cell discharges, but they were elicited by thalamic and antidromic stimulation and were in phase with dendritic activity.

The postsynaptic activity of pyramidal cells produces a *current dipole*. When an excitatory postsynaptic potential takes place, current enters into the cell at some point in the somatodendritic compartment and, as a necessary consequence, current must exit the cell at distant locations. The opposite occurs when an inhibitory postsynaptic potential is elicited. The currents that are produced away from the active postsynaptic sites are called *return currents*. The zone where current enters

the cell is called a *sink*, and the zone where current exits the cell is called a *source* (Buzsáki et al., 2012; Nunez and Srinivasan, 2006) (Figure 1.1). The current dipoles generated by pyramidal cells have been dubbed *open fields*, following the description of Lorente De Nó (1947), because it "permits the spread of the current in the volume of the brain". This dynamic of concurrent current source and sink constitutes a current dipole. These current dipoles generate current waves that are conducted through the brain, skull and scalp until they reach the electrodes, producing the signals in the EEG recordings (Nunez and Srinivasan, 2006).

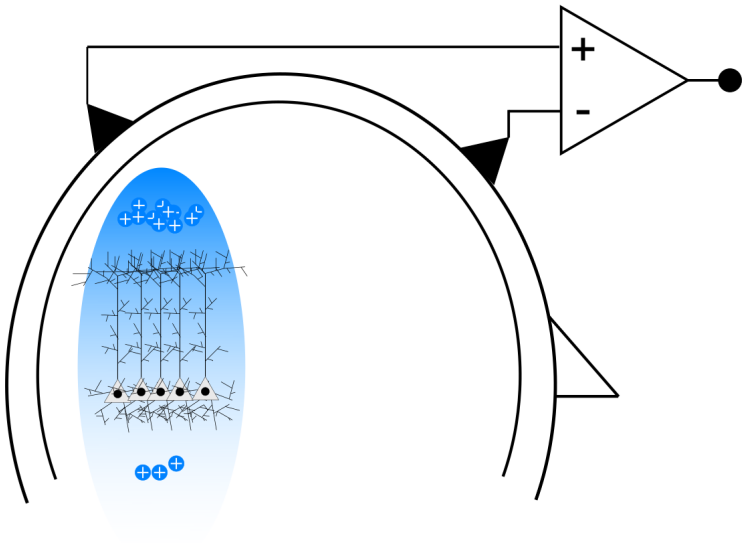

Figure 1.1: Cortical dipole generation. Cortical dipoles are generated by the concurrent activity of pyramidal cells. Sites where current enters into the cells are named sinks (light blue background), and points where current exits the cells are named sources (dark blue background). The activity of individual cells add up to generate a macroscopic dipole, whose polarity is defined by the type of synapse involved.

On the contrary, subcortical sources are considered to contribute very little to the EEG signal (Attal et al., 2012; Nunez and Srinivasan, 2006). This is substantiated by

at least two different characteristics of subcortical sources. First, subcortical sources are located relatively away from the scalp surface. Concurrent recordings using intracortical and scalp electrodes have showed that intracortical currents are attenuated in their way to the scalp (Cooper et al., 1965). Thus, subcortical structures produce much smaller EEG signals compared to neocortical sources. Additionally, some subcortical sources have cytoarchitectures that make them produce *closed fields*, as opposed to the open fields previously described. Theoretically, these closed fields produce voltages $V = 0$ outside the structure (Klee and Rall, 1977). Closed fields are formed when neurons are arranged radially. For instance, the superior olive preferentially contain somata in the periphery of the nucleus and dendrites in the central region. When superior olive neurons are active, most of the current arising from the current dipoles stays inside the structure (Lorente De Nó, 1947). In recent years, however, some researchers have presented evidence for the presence of subcortical activity in EEG signals, relying on tools such as high density EEG (Seeber et al., 2019) or newly developed algorithms (Krishnaswamy et al., 2017).

The electrical activity measured at the scalp results from the summed activity of numerous neurons. This summation is brought about by both spatial and temporal variables. When pyramidal cells in a gyrus are stimulated, the current dipoles they generate add up together producing a radial dipole whose magnitude is sufficiently large to be measured at the scalp. Similarly, neurons located in sulci and fissures form tangential dipoles but their orientation and depth produce a lower signal compared to radial dipoles (Nunez and Srinivasan, 2006). Cooper et al. (1965) suggested that

at least a cortical area of 6 $[cm^2]$ is necessary to produce a measurable signal, but later studies have reported estimations ≈ 4 $[cm^2]$ (as reviewed by Riera et al., 2012). Additionally, current dipoles can be summed in time. While n synchronous neurons generate a signal whose magnitude is proportional to n, a signal emerging from n asynchronous neurons has a magnitude proportional to $\sqrt{n}$ (Elul, 1972). Overall, spatial and temporal summation generate voltage signals in the range of 10-100 $[\mu V]$ at the scalp surface of a normal individual (Niedermeyer, 2005b).

1.2 Temporal EEG dynamics

The temporal dynamics of the underlying neural populations that give birth to the EEG signal has been a focus of research since Lord Adrian's seminal work on the human alpha rhythm. Adrian interpreted that the emergence of the alpha rhythm is triggered by the synchronized activity of the underlying neural population (Adrian and Matthews, 1934a; Hodgkin, 1979). This claim became the standard interpretation for EEG phenomena (Pfurtscheller and Lopes da Silva, 1999; Rao and Edwards, 2008), and thus the existence of EEG signals emerging from asynchronous populations has been constantly dismissed in the EEG field (see for instance Cohen, 2017). Nonetheless, since the 1960s, researchers in the West began to think that the EEG signal may be the random addition of elementary oscillators, a formulation that requires the EEG signal have some properties of Gaussian noise. Additionally, arrhythmic EEG activity, non-Gaussian signals that do not present periodicity, have

only recently received attention and studied in the context of the greater framework of scale-invariant (scale-free) phenomena (He, 2014).

1.2.1 Brain waves

Brain waves — also called brain oscillations or brain rhythms — are rhythmic, periodic EEG patterns that are considered to emerge from synchronous activity in neocortex patches (Steriade et al., 1990). Being rhythmic, these signals present a distinctive periodic, sinusoidal morphology and are thought to be exclusively associated with peaks in the spectral profile (Buzsáki et al., 2013). The origin of brain waves is attributed to both single neuron features and brain network dynamics. At the cellular level, extensive *in vitro* and *in vivo* evidence shows that pyramidal and thalamic cells oscillate at preferred frequencies due to the conductances present in their somatodendritic and axonal compartments. These cells also present resonance: they respond preferentially to presynaptic trains of specific frequencies (Hutcheon and Yarom, 2000; Llinás, 1988). In addition, there are two main hypothesis that explain the origin of EEG brain waves from networks of neuronal elements: thalamocortical and cortico-cortical networks. Some brain waves have been shown to be produced by thalamocortical projections from pacemaker cells. The delta rhythm, a 1-4 [Hz] pattern observed during NREM sleep, is produced in the neocortex by influence of thalamic cells that intrinsically oscillate at frequencies in the same band (Steriade et al., 1993a). Slow oscillations, a rhythmic signal of frequency <1[Hz], appear concurrently with delta waves during NREM sleep. Nevertheless, this signal

is immune to thalamic ablation, and thus it is believed to be originated by cortico-cortical networks (Steriade et al., 1993b; Steriade et al., 1993c). As a first theoretical approximation, brain waves have been proposed to emerge from the synchronous activity of a population of coupled oscillators (Breakspear et al., 2010).

1.2.2 Gaussian EEG signals

Gaussian EEG signals correspond to signals whose amplitude values follow a Gaussian distribution. Theoretically, Gaussian signals also display a broadband, flat spectrum, and therefore have been named *white Gaussian noise* (WGN) (Schwartz et al., 1995). This class of signals have only been sporadically reported in the EEG literature. In a pioneer study, Elul (1969) studied 2[s] epochs recorded either in an idle state or during a mental arithmetic task. He calculated the experimental amplitude probability distribution of these epochs and compared it with the Gaussian distribution using the chi-square goodness of fit test, finding a closer fit during the idle state than during the mental task. Additional tools such as Kolmogorov-Smirnov test or autoregressive models have been used with varying results (Gonen and Tcheslavski, 2012; McEwen and Anderson, 1975). Nevertheless, as Gaussian signals emerge from asynchronous populations (Elul, 1969), the existence of those signals has been constantly disregarded under the assumption that the amplitude of a signal emerging from such a population is either zero or, at best, too weak to be measured at the scalp (Cohen, 2017; Elul, 1972; Lachaux et al., 1999; Singer, 1999). On the contrary, formal analysis shows that the signals emerging from a population

of asynchronous oscillators have an amplitude proportional to $\sqrt{n}$ (Elul, 1972); a fact that was pointed out early in the EEG literature by Dr. Koiti Motokawa (Motokawa and Mita, 1942; Motokawa, 1943; Tasaki, 1971) but was ignored as Motokawa's work was published in German in a Japanese journal during World War II (Díaz et al., 2018; Rao and Edwards, 2008). Thus, EEG Gaussianity reports are interesting as they call into question mistaken notions about signal generation and pave the way to study the functions of asynchronous populations in brain dynamics.

1.2.3 Arrhythmic EEG

EEG signals display a spectrum that contains a well-known broadband *1/f* component described by a power-law function $1/f^{\beta}$ (linear after logarithmic transformation), where β is called the power-law exponent. As this function is characteristic of scale-invariant (or scale-free) dynamics which have no distinctive temporal scale (Khaluf et al., 2017), signals contributing to the 1/f spectral component have been dubbed *arrhythmic EEG signals* (He, 2014). Signals with distinctive sharp-edged waveform display a broadband *1/f* spectral profile (Kramer et al., 2008). Unfortunately, these signals were first recognized in the field of electronics as "flicker noise" (Milotti, 2002), and thus scale-invariant brain signals have been historically disregarded as instrumental noise (He, 2014). Experimental evidence, however, shows that the power-law exponent of EEG signals varies under different behavioral conditions (Dehghani et al., 2010) and anesthetics (Colombo et al., 2019), suggesting that arrhythmic EEG signals are not noise but reflect relevant underlying brain processes.

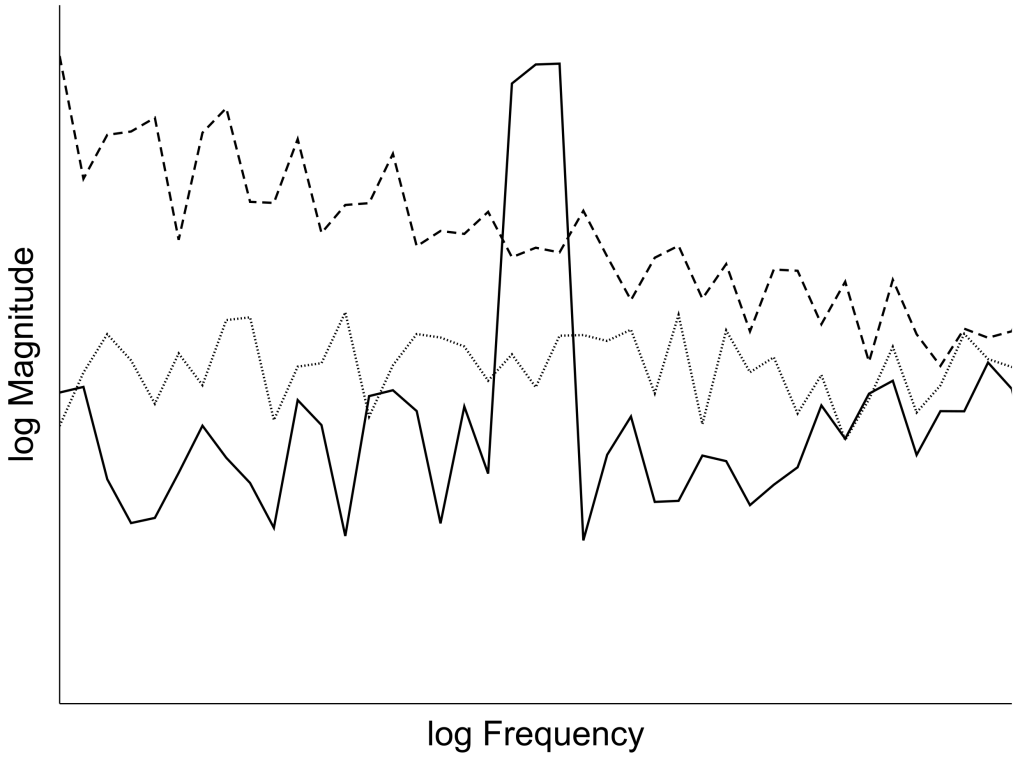

Figure 1.2: Spectral profiles of temporal EEG dynamics. Temporal EEG dynamics can be characterized in the frequency domain by their spectral profiles. Notice that both axes are log-transformed. Brain waves are considered to be exclusively connected to peaks in the spectrum (solid trace). Broadband Gaussian signals display a flat spectrum (dotted trace), and arrhythmic or scale-invariant signals show a *1/f* profile that appears linear after logarithmic transformation (dashed trace).

1.3 Temporal EEG models: weakly coupled oscillators systems

A system of *weakly coupled oscillators* (WCO) consists of a population of limit-cycle oscillators that vibrate at their own natural frequencies and weakly interact with each other (i.e. they are coupled) (Izhikevich and Kuramoto, 2006). WCO models are particularly relevant to study EEG signal generation as they have been

widely used to model cortical activity (Breakspear et al., 2010; Schultheiss et al., 2012). Limit-cycle oscillators are self-sustained, dissipative entities that display a distinctive period, amplitude and waveform (Winfree, 1967). In other words, their trajectories form a closed loop in phase space (x, dx/dt) and return to it even after an external perturbation. Since oscillators are weakly coupled, the system does not significantly alter the limit-cycle of each oscillator. Nonetheless, as a whole the entire system can display different dynamics depending on the coupling strength and the distribution of the natural frequencies. These behaviors include synchrony, where all oscillators reach the same frequency, as well as asynchrony, where all oscillators vibrate independently (Strogatz, 2018). The famous cybernetician Norbert Wiener was the first researcher to study mathematically the collective behavior of a population of WCO, linking synchronization dynamics to the neural mechanism underlying the human alpha rhythm (Strogatz, 1994; Wiener, 1948). Nonetheless, Dr. Arthur Winfree was the first to propose a model of WCO to explain the rhythmic behavior of biological phenomena such as heart pacemakers or fireflies' synchronized flashing (Winfree, 1967).

1.3.1 Kuramoto model

The *Kuramodo model* is a WCO model proposed by Dr. Yoshiki Kuramoto (Kuramoto, 1975). Inspired by Dr. Winfree's work (Kuramoto and Nishikawa, 1987), Kuramoto proposed a model that consists of a system of limit-cycle phase oscillators, where each phase oscillator θ is represented by the following ordinary differential

equation (Strogatz, 2000):

$$\dot{\theta}_i = \omega_i + \frac{K}{N}\sum_{j=1}^{N} sin(\theta_j - \theta_i) \ , \ i = 1, ..., N \tag{1.1}$$

Where:

$\dot{\theta}_i$ = the first time derivative of the ith oscillator.

ω_i = the natural frequency of the ith oscillator.

K = the coupling constant.

N = the total number of oscillators.

In this model, each oscillator vibrates with constant amplitude at its own natural frequency ω_i, while the entire system follows a distribution of frequencies $g(\omega)$. Additionally, each oscillator interacts with all others in an all-to-all coupling proportional to the coupling constant K and to the sine of the phase difference between oscillators by the term $\sum_{j=1}^{N} sin(\theta_j - \theta_i)$. The collective behavior of the whole system can be characterized by its centroid vector, also known in this context as the order parameter (ibid.):

$$re^{i\psi} = \frac{1}{N}\sum_{j=1}^{N} e^{i\theta j} \tag{1.2}$$

Where:

r = the amplitude envelope of the order parameter.

ψ = the phase of the order parameter.

N = the total number of oscillators.

Remarkably, each oscillator's equation (Equation 1.1) can be re-written to re-

place the all-to-all interaction term $\frac{K}{N}\sum_{j=1}^{N} sin(\theta_j - \theta_i)$ using the order parameter (Strogatz, 2000):

$$\dot{\theta}_i = \omega_i + Kr * sin(\psi - \theta_i) \ , \ i = 1, ..., N \tag{1.3}$$

In this expression, it can be seen that all oscillators are coupled with each other implicitly and the order parameter pulls the phase of all oscillators towards its own phase ψ (ibid.); a phenomenon known as the slaving principle (Haken, 1996).

The Kuramoto model exhibits three different population regimes: frequency locking, partial locking, and incoherence. These regimes arise depending on the natural frequency distribution and the coupling constant of the population. For a given frequency distribution $g(\omega)$, there is a critical coupling value K_c (Strogatz, 2000):

$$K_c = \frac{2}{\pi g(0)} \tag{1.4}$$

Thus, for coupling constant values $K < K_c$, oscillators are uncoupled and oscillate at their own natural frequencies. Hence, the system follows the incoherence regime. For $K \approx K_c$ the system enters into partial synchronization. Many oscillators synchronize, while others oscillate independently. As K increases further, more and more oscillators are recruited and the system becomes fully locked (Acebrón et al., 2005). For this reason, the amplitude envelope of the order parameter r becomes a measure of coherence in the system. When $r \to 1$, oscillators tend to be totally

in-phase and the entire system is fully synchronized. Conversely, when r revolves around values closer to 0, oscillators tend to vibrate at their own natural frequencies and the system behaves asynchronously (Strogatz, 2000). The Kuramoto model is a key framework in the EEG field because of its potential to simulate cortical oscillations, and thus has been extended to introduce more biologically-oriented features (such as bi-dimensional arrangements) that make it a better model for brain dynamics (Breakspear et al., 2010; Cumin and Unsworth, 2007). In fact, Dr. Kuramoto himself highlighted that the order parameter during a synchronized regime displays a spectrum similar to the human alpha rhythm's (Kuramoto, 1975).

1.3.2 Matthews–Mirollo–Strogatz model

The *Matthews–Mirollo–Strogatz model* (MMS model) is a system of WCO where each element is a limit-cycle oscillator of varying phase and amplitude. Each oscillator z is described in the complex plane by the following ordinary differential equation (Matthews et al., 1991; Matthews and Strogatz, 1990):

$$\frac{dz_j}{dt} = (1 - |z_j|^2 + i\omega_j)z_j + \frac{K}{N}\sum_{i=1}^{N}(z_i - z_j) \tag{1.5}$$

Where:

dz_j/dt = the first time derivative of the jth oscillator.

ω_j = the natural frequency of the jth oscillator.

K = the coupling constant.

N = the total number of oscillators.

Each oscillator z in this model varies in amplitude and phase in the complex plane at its own natural frequency ω, while the frequencies of all oscillators follow a distribution $g(\omega)$ with bandwidth Δ. Also, every oscillator is coupled with all others by the term $\frac{K}{N}\sum_{i=1}^{N}(z_i - z_j)$. As in the Kuramoto model, the behavior of the entire system can be described by the order parameter as (Matthews et al., 1991):

$$\overline{z} = Re^{i\phi} = \frac{1}{N}\sum_{j=1}^{N} z_j \tag{1.6}$$

Where:

R = the amplitude envelope of the order parameter.

ϕ = the phase of the order parameter.

N = the total number of oscillators.

The equation for each oscillator (Equation 1.5) can be re-written using the order parameter as (ibid.):

$$\frac{dz_j}{dt} = (1 - |z_j|^2 + i\omega_j)z_j + K(\bar{z} - z_j) \tag{1.7}$$

Again, all oscillators are coupled with each other through the order parameter.

The MMS model displays several distinctive regimes depending on both the coupling constant K and the bandwidth Δ of the frequency distribution $g(\omega)$. Stable states (as $time \to \infty$) include, as in the Kuramoto model, frequency locking, partial locking and incoherence. Also, a novel fourth stable state appears: amplitude death, where oscillators are tightly coupled, the bandwidth of the system is relatively high, and the order parameter ends up having an amplitude equal to 0. In addition, several unsteady states exist for a subset of K and Δ (Matthews et al., 1991). Thus, the MMS model contains all behaviors present in the Kuramoto model. In fact, the Kuramoto model happens to be a particular case of the MMS model (ibid.). The MMS model has also been applied to the study of neural processes (Díaz et al., 2007; Rudrauf et al., 2006).

1.4 Human Alpha Rhythm

The *human alpha rhythm* is a EEG signal of variable frequency in the range 8-13 [Hz], which appears when individuals are wakeful and resting with the eyes closed and disappears when the eyes are open or under attentional processes. Thus, the alpha rhythm is considered to be a *resting-state electroencephalography* (rs-EEG) phenomenon. This signal can be recorded in the occipital area of the scalp with a magnitude usually under 50 $[\mu V]$ (Kane et al., 2017). The alpha rhythm was first described by Dr. Berger himself (see Figure 1.3) (Berger, 1929) but his report failed to produce widespread interest and acceptance (Gloor, 1969). Only after Adrian and

Matthews (1934a) published a thorough examination of the phenomenon this signal was accepted by the scientific community (see Figure 1.4). In fact, these authors' report describes the most important features of the human alpha rhythm.

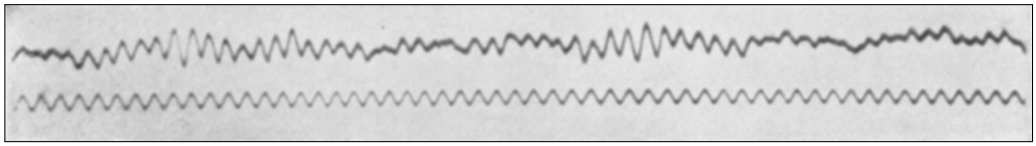

Figure 1.3: Dr. Hans Berger's alpha rhythm recordings. Upper trace: Alpha rhythm signal. Lower trace: base time 10 [Hz]. Extracted from Berger (1929) with permission.

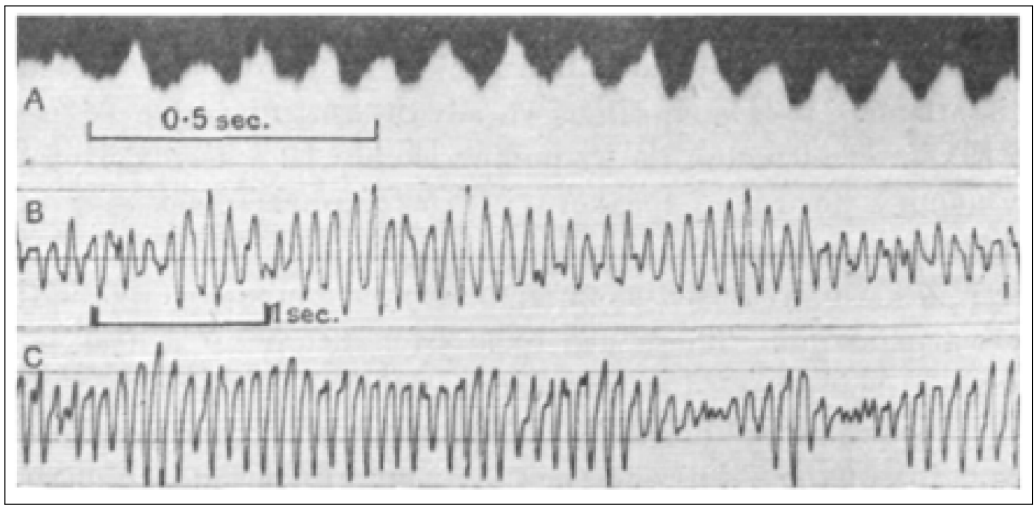

Figure 1.4: Lord Adrian's alpha rhythm recordings. Extracted from Adrian and Matthews (1934a) with permission.

1.4.1 Interindividual differences

Differences among individuals have been reported for some characteristics of the alpha rhythm. First of all, some individuals may simply not present alpha rhythm, a feature reported early in Lord Adrian and Matthews' work. While Adrian had a normal alpha rhythm, this signal was seldom obtained if not at all in Matthews'

recordings (Adrian and Matthews, 1934a). The magnitude of the rhythm is variable, and values from 5 to 100 [μV] have been reported for different subjects (Niedermeyer and Lopes da Silva, 2005, p. 169). Moreover, differences have been found in the amplitude modulation of the rhythm. Adrian and Matthews described that the alpha rhythm follows a characteristic regime of temporal power fluctuation and named this behavior "waxing and waning" or "pulsating" activity. Nonetheless, Davis and Davis (1936) reported as many as four distinct amplitude modulation patterns distinguishable by time percentage of alpha power presence. Contrary to Adrian and Matthews' results, these authors report a modulation regime where little or no waning is present. This variety of amplitude modulation regimes has been described by several researchers as well (Mimura, 1971; Niedermeyer and Lopes da Silva, 2005, p. 171; Schroeder and Barr, 2000).

1.4.2 Neural Generator

The generator of the alpha rhythm is located in the occipital area of the cortex. Adrian and Matthews offered evidence for the intracranial origin using several controls. A possible origin from eyes movements was dismissed by recording from scalp electrodes under different ocular tasks. In the same line, the activity from facial and neck muscles was discarded due to the absence of the target signal under changes of posture and muscular contraction (Adrian and Matthews, 1934a). In addition, evidence in favor of the cortical origin was provided by spatial screening of the signal magnitude on both normal and trephined individuals. Also, electrodes placed

on the occipital region of the scalp were found to provide the maximum magnitude values (Adrian and Matthews, 1934a). Then, Adrian and Yamagiwa (1935) further explored the signal topography by spatial screening along the sagital and transverse planes. Using just 4 electrodes, they reported that in fact there are two alpha generators in the occipital area, one generator in each hemisphere. This result was later supported by multichannel EEG data (Lehmann, 1971). *Intracranial electroencephalography* (iEEG) studies in dogs have reported that the most uncontaminated and strongest alpha rhythm signals can be recorded from the mesial surface of the occipital lobe, over the calcarine cortex (Lopes da Silva et al., 1973), and that the alpha rhythm generator corresponds to a dipole whose center is located near layer V of the visual cortex (Lopes da Silva and Van Leeuwen, 1977).

1.4.3 Generator dynamics

The dynamics of the alpha rhythm generator has not been completely elucidated. Adrian and Matthews described that the rhythm's natural frequency can be modified by direct stimulation of the retina using a flickering light field of the desired new frequency and reported successful induction to frequencies between 7-25[Hz], a result that has been replicated by others as well (Gebber et al., 1999; Toman, 1941). These features, together with the high energy of the signal, led Adrian and Matthews to propose that the alpha rhythm emerges from a group of neurons beating synchronously, while its fading when the eyes are opened reflects a change into a asynchronous regime (Adrian and Matthews, 1934a). This synchrony/asynchrony

interpretation has permeated the field ever since, and today it has been conceptualized as *event-related synchronization* (ERS) and *event-related desynchronization* (ERD) (Pfurtscheller and Lopes da Silva, 1999). In the same line, the famous cybernetician Norbert Wiener suggested that the alpha rhythm generator behaves as a synchronized population of nonlinear coupled oscillators (Strogatz, 1994; Wiener, 1948).

Nevertheless, some authors have found Gaussian characteristics in the alpha rhythm signal. Saunders (1963) studied "well-developed" epochs of alpha rhythm and compared the experimental distribution of the magnitude values to the Gaussian distribution and found a close similitude. Similarly, Dick and Vaughn (1970) relied on alpha rhythm epochs but examined the envelope of each segment, which was estimated by the complex demodulation method (Ktonas and Papp, 1980). They compared the distribution of the magnitude values of the envelope to the Rayleigh distribution and found a close fit. The Rayleigh distribution describes the magnitude of the envelope of a Gaussian signal (Schwartz et al., 1995). This type of evidence led some researches to propose that the alpha rhythm generator may be regarded as an alpha filter (Lopes da Silva et al., 1973). In other words, the alpha rhythm generator would receive WGN input and would filter it in the alpha band. This interpretation of the generator as a narrowband bandpass filter can be traced back to Prast (1949).

1.5 Envelope Analysis

The *envelope analysis* of a signal $s(t)$ relies on the study of its *envelope function* (also known as amplitude envelope) and the *coefficient of variation of the envelope* (CVE) to characterize the dynamics of the population of unitary elements that generates it. The envelope function $A(t)$ receives its name because it actually "envelops" the signal $s(t)$ (Figure 1.5), thus representing the instantaneous amplitude of $s(t)$, and is calculated using the *Hilbert transform* (HT) as (Cohen, 1995):

$$A(t) = \sqrt{s^2(t) + H[s(t)]^2} \tag{1.8}$$

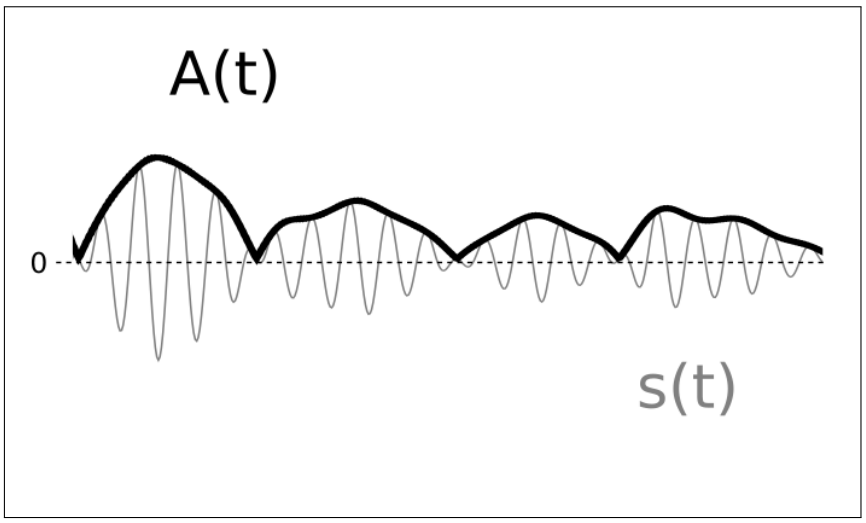

Figure 1.5: Envelope function. The signal $s(t)$ (grey trace) and its envelope $A(t)$ (black trace) are shown. The envelope function is the instantaneous amplitude of $s(t)$. Notice how $A(t)$ follows the local maxima of $s(t)$ over time enveloping $s(t)$. Notice also that $s(t)$ is a zero-mean signal, and thus its coefficient of variation is not defined. On the other hand, the envelope $A(t)$ is always non-negative and its coefficient of variation can be calculated.

This method was developed by Díaz et al. (2018) relying on rat EEG and capitalizing on previous work done by Díaz et al. (2007) in vertebrate olfactory epitelium. Thus, the envelope analysis was introduced as *EEG envelope analysis* (EnvEEG), which is the interpretation adopted in this work as well. Nevertheless, it is worth noting that applications in other research fields are yet to be explored.

A signal generated by the sum of a large number of independent variables should have the characteristics of WGN (Elul, 1972). This signal exhibits unique features. In particular, the CVE of a continuous-time zero-mean WGN signal is equal to $\sqrt{(4-\pi)/\pi}$ (Schwartz et al., 1995). Therefore, this parameter can be used as a *fingerprint of Gaussianity* to evaluate if a particular signal is produced by a population of asynchronous oscillators. As previously mentioned in section 1.2, the possibility of detecting Gaussianity is of great importance in EEG as asynchronous signals have been repeatedly dismissed in the field. Nonetheless, the CVE for discrete-time zero-mean WGN is not unique and its distribution must be calculated *in silico*. This distribution allows making a 99% confidence interval to assess the null hypothesis of Gaussianity as $H_0 : CVE = CVE_{Gaussian}$. Thus, any deviation from Gaussian CVE is connected with different non-Gaussian, and therefore synchronous dynamics. Additionally, the *mean of the envelope* (ME) is also measured to estimate signal energy. CVE and ME represent two fundamental signal parameters and can be combined to produce a new phase-space: the *envelope characterization space* (EnvSpace). This space unifies generator dynamics, energy and signal morphology in a single framework for EEG signal classification (Díaz et al., 2018).

1.5.1 CVE for ideal signals

Gaussian signals

From a statistical point of view, a stationary signal $s(t)$ produced by the sum of a large number of independent variables follows a Gaussian distribution with mean equal to zero and variance σ^2 (Cramér, 1970). This signal is known as WGN and its *probability density function* (PDF) is (Schwartz et al., 1995):

$$p(x) = \frac{1}{\sqrt{2\pi\sigma^2}} e^{\frac{-x^2}{2\sigma^2}} \tag{1.9}$$

WGN displays a flat spectrum and its envelope exhibits a particular PDF, which can be derived analytically (ibid.). To calculate the PDF for the envelope of a Gaussian signal, first the HT of the signal must be calculated. Given that the HT is a linear operator (King, 2009, p. 145), and that the result of a linear operation on a Gaussian random variable is itself a Gaussian random variable, $H[s(t)]$ follows a Gaussian PDF with equal mean and variance. Additionally, the signal and its HT are independent (Schwartz et al., 1995). Thus, following the definition of envelope in Equation 1.8, it can be seen that the PDF for the envelope function is $\sqrt{x^2 + y^2}$ being x and y two independent zero-mean Gaussian random variables. This distribution corresponds to the Rayleigh distribution (Papoulis and Pillai, 2002):

$$p(x) = \frac{x}{\sigma^2} e^{\frac{-(x)^2}{2\sigma^2}} \tag{1.10}$$

The coefficient of variation for the entire family of Rayleigh distributions is $\sqrt{(4-\pi)/\pi}$ (Papoulis and Pillai, 2002, p. 162), and it corresponds to the CVE of the envelope of a zero-mean WGN signal. This value holds for both white noise and any of its filtered bands (Schwartz et al., 1995). This result, however, does not hold for discrete WGN of arbitrary length. Therefore, the envelope analysis of discrete signals (such as EEG) requires the *in silico* estimation of the CVE probability density function for discrete WGN (Díaz et al., 2018).

CVE for weakly coupled oscillators systems

In exploring the validity of CVE in the study of neural dynamics, Díaz et al. (2007) studied the CVE of signals generated from simulations of both the Kuramoto model and the MMS model in order to evaluate the CVE as a signal descriptor. In the process, they executed a screening of the MMS model phase space and reported that the CVE characterized each type of behavior emerging from this model.

Asynchronous signals showed CVE values similar to WGN. The researchers simulated a Kuramoto system of 25 oscillators in a frequency band equal to $30 \pm 1.5[Hz]$. Incoherence in the system was induced setting the coupling value K to zero, finding that the CVE of the resultant signal varied closely around ≈ 0.523. For asynchronous signals coming from the MMS model, they reported that the CVE stays close to 0.523 even though this model allows for variations in amplitude.

Deviations from Gaussianity were also characterized by CVE. Low-CVE signals were found to emerge from phase-locking dynamics. In their Kuramoto model sim-

ulation, the researchers set the coupling constant K to increasing values, which consistently produced lower CVE values as the coupling constant K increased. The MMS model screening linked low-CVE values to phase-locking as well. High-CVE values were found during simulations of the MMS model only and were linked to unsteady behaviors that emerge from combinations of medium coupling constant K and bandwidth Δ. These high-CVE signals were characterized by pulsating or phasic morphologies.

1.5.2 Implementation

The envelope function is obtained from the calculation of the *analytic representation* of the signal. The analytic signal of $s(t)$, denoted here as $z(t)$, is a complex representation of a real-valued signal and was introduced by Gabor (1946). In this representation, the real part is the signal $s(t)$ itself, while the imaginary part is the HT of the signal:

$$z(t) = s(t) + jH[s(t)] \tag{1.11a}$$

$$= z_{Real}(t) + jz_{Imag}(t) \tag{1.11b}$$

Where the second term $H[s(t)]$, the Hilbert transform, applies a shift of $\frac{\pi}{2}$ to every negative frequency component and a shift of $-\frac{\pi}{2}$ to every positive frequency component, and it is calculated as a Cauchy principal value (King, 2009):

$$H[s(t)] = \frac{1}{\pi} P \int_{-\infty}^{\infty} \frac{s(y)}{t-y} dy \tag{1.12}$$

Alternatively, the analytic signal can be expressed in the frequency domain as a piecewise function based on the *Fourier transform* (FT) of $s(t)$, denoted as $\hat{s}$. $\hat{z}(\omega)$ is defined as follows (Marple, 1999):

$$\hat{z}(\omega) = \begin{cases} 2\hat{s}(\omega) & for\ f > 0 \\ \hat{s}(\omega) & for\ f = 0 \\ 0 & for\ f < 0 \end{cases} \tag{1.13}$$

As the analytic signal is a complex signal, it can be expressed using polar coordinates and the Euler's formula as:

$$z(t) = A(t)e^{j\phi(t)} \tag{1.14}$$

Where $A(t)$ is the envelope (or amplitude envelope) function and $\phi(t)$ is the phase function and are calculated as (Cohen, 1995, p. 27):

$$A(t) = \sqrt{s(t)^2 + H[s(t)]^2} = \sqrt{z_{Real}(t)^2 + z_{Imag}(t)^2} \tag{1.15a}$$

$$\phi(t) = \arctan\left(\frac{H[s(t)]}{s(t)}\right) = \arctan\left(\frac{z_{Imag}(t)}{z_{Real}(t)}\right) \tag{1.15b}$$

Then, the coefficient of variation of the envelope is calculated as the standard deviation divided by the mean:

$$CVE = \frac{\sigma_{A(t)}}{\mu_{A(t)}} \tag{1.16}$$

As EEG signals are analyzed as discrete representations of continuous physiological signals, EnvEEG requires discrete implementations of the previously described operations. A continuous signal $s(t)$ sampled with frequency f results in a discrete signal $s[n] = s(nT)$, where $T = \frac{1}{f}$. The discrete analytic representation is here denoted as $z[n]$. To obtain this new signal, one could be tempted to calculate the discrete Hilbert transform of $s[n]$, which is defined as (King, 2009, p. 660):

$$H_D[s[n]] = \frac{1}{\pi} \sum_{m=-\infty}^{\infty} \frac{s[m]}{n-m} \quad , m \neq n \tag{1.17}$$

Nevertheless, the calculation of $z[n]$ is usually implemented in the frequency domain using the *discrete Fourier transform* (DFT), due to computational efficiency. This procedure uses the Fast Fourier Transform, an algorithm for fast DFT computation, and follows the definition of the analytic signal expressed in Equation 1.13. Essentially, the procedure calculates the DFT of the discrete signal $s[n]$, "sets to zero" the values for the negative frequencies of $\hat{s}[n]$, and doubles the values for the positive frequencies. Afterwards, it computes the *inverse discrete Fourier transform* (IDFT) of the "modified" $\hat{s}[n]$, obtaining the discrete analytic representation $z[n]$ (Marple, 1999).

With $z[n]$ at hand, the discrete envelope(or amplitude envelope) function of $s[n]$ is defined as:

$$A[n] = \sqrt{z_{Real}[n]^2 + z_{Imag}[n]^2} \tag{1.18}$$

It must be stated, however, that the use of DFT-IDFT computation includes intrinsic errors in the estimation of $z[n]$. As a consequence, this procedure introduces spurious effects at both ends of the envelope function (Luo et al., 2009). Then, as in Equation 1.16, the coefficient of variation of the discrete envelope is calculated as:

$$CVE = \frac{\sigma_{A[n]}}{\mu_{A[n]}} \tag{1.19}$$

Additionally, to apply the envelope analysis to EEG signals, some extra procedures must be included before the envelope calculation. EEG signals are traditionally classified into different frequency sub-bands, and many phenomena can only be properly characterized once they are isolated in the frequency domain. Thus, the signal must be filtered in accordance with the actual phenomenon under study (Niedermeyer, 2005b). To account for EEG nonstationarity, an approximation of stationarity is also implemented by epoching the signal into segments of arbitrary length (Barlow, 1985); a widely applied strategy in EEG signal processing (Mitra and Pesaran, 1999). Then, the subsequent envelope analysis is applied to each segment, which produces a bivariate time series of CVE and ME values. This time series enables the monitoring of the time-variant dynamics of the envelope parameters and are used to create the envelope characterization space. The basic pipeline for EnvEEG

implementation is shown in Figure 1.6. Finally, since the value $\sqrt{(4-\pi)/\pi}$ only holds for continuous WGN, the CVE distribution of filtered and discrete zero-mean WGN must be calculated to assess Gaussianity. This surrogate data is obtained by numerical simulations and depends on three parameters: epoch length, bandwidth, and sampling frequency. These parameters must be set equal to the empirical parameters values during the simulation, which involves the following steps:

1. Take *epoch length* $*$ *sampling rate* samples from $\mathcal{N}(0,\, \sigma^2)$ to obtain a simulated discrete WGN epoch.

2. Filter the WGN epoch in the desired bandwidth using the same filter applied to the experimental data.

3. Calculate the envelope of the filtered WGN epoch.

4. Remove both tails of the envelope (to control for spurious effects) and calculate the CVE.

5. Repeat steps 1, 2, 3, and 4 a million times to approximate the PDF for the CVE of discrete zero-mean WGN.

Note that Díaz et al. (2018) also used Fourier transform phase randomization (Theiler et al., 1992) to simulate the CVE distribution, but they obtained similar results and opted for the procedure just delineated. From this distribution, a $1-\alpha\%$ confidence interval for a given significance value α is created to assess the null hypothesis $H_0 : CVE_{epoch} = CVE_{Gaussian}$, and three different CVE classes

are established: low-CVE ($CVE < \alpha/2$), mid-CVE ($\alpha/2 \leq CVE \leq \alpha/2$), and high-CVE ($\alpha/2 < CVE$). Additionally, these three CVE classes feature distinctive morphologies: rhythmic (low-CVE), Gaussian (mid-CVE), and phasic (high-CVE) (see Figure 1.7).

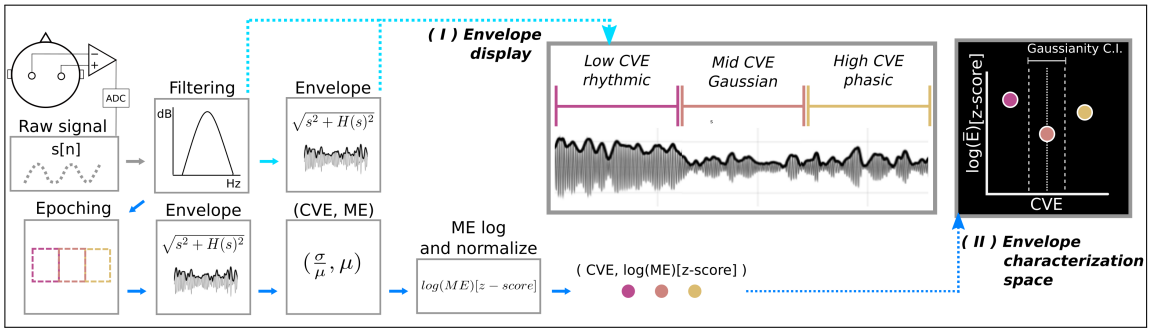

Figure 1.6: EEG envelope analysis basic pipeline. After the signal is digitized and filtered as needed, the data follow two parallel paths. **(I)** The envelope is calculated for the whole signal and both are displayed to visualize amplitude, amplitude modulation and signal morphology. **(II)** The data is divided in epochs and the envelope is calculated for each epoch. Then, the coefficient of variation of the envelope (CVE) and the mean of the envelope (ME) are calculated. The ME is log-transformed and normalized. Finally, the (CVE,log(ME)[z−score]) points are plotted in the envelope characterization space. Note that the whole pipeline can be used for all traditional EEG sub-bands independently.

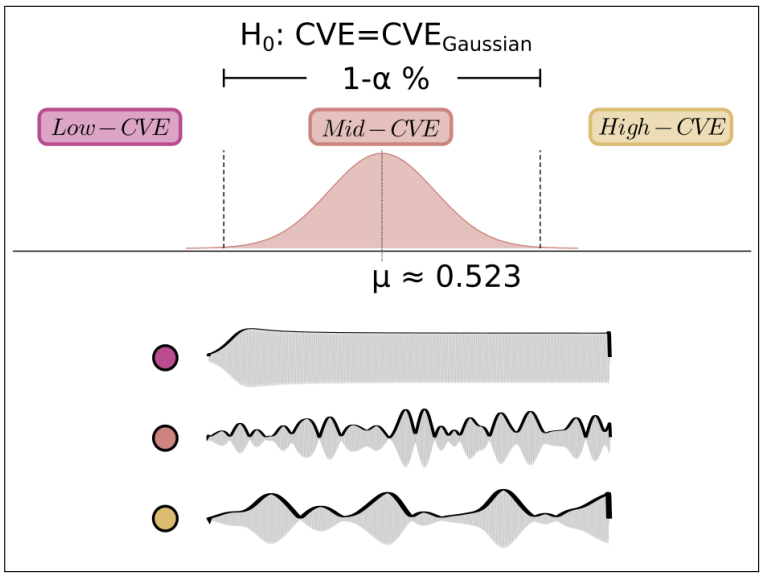

Figure 1.7: Gaussian CVE distribution, CVE classes, and their distinctive morphologies. The CVE distribution for discrete white Gaussian noise is obtained *in silico*. The Gaussian CVE distribution allows making a 1-α% confidence interval to assess the null hypothesis of Gaussianity (α is the significance level). Dashed lines mark the lower and upper limits of the Gaussianity confidence interval, and the dotted line shows the mean of the surrogate distribution (approximately $\sqrt{(4-\pi)/\pi}$). Thus, three CVE classes are established: low-CVE (purple), mid-CVE (salmon), and high-CVE (gold). CVE classes are characterized by distinctive signal morphologies. Low-CVE signals (upper trace) are synchronous, wave-like signals, while mid-CVE signals (middle trace) display a Gaussian noise profile. High-CVE signals (lower trace) are synchronous, non-sinusoidal but phasic and resemble pulsating ripples.

1.5.3 Envelope characterization space

The envelope characterization space is a 2D phase space composed of the coefficient of variation of the envelope and the mean of the envelope, which represent two fundamental aspects of the signal: morphology (CVE) and energy (ME). Since the CVE is a dimensionless parameter, it is relevant to explore how CVE and ME correlate. Ideally, the values of ME must be log-transformed and normalized to account for setup diversity. The CVE is also linked to different generator dynamics.

Low-CVE values have been shown to emerge from frequency-locking dynamics in weakly coupled oscillators models, while mid-CVE values represent white Gaussian noise. High-CVE values have been shown to emerge from unsteady states in weakly coupled oscillator systems. Thus, the EnvSpace condenses generator dynamics, energy, and signal morphology in a single framework. The $1 - \alpha\%$ confidence interval of Gaussianity is also included. An schematic of the envelope characterization space is shown in Figure 1.8.

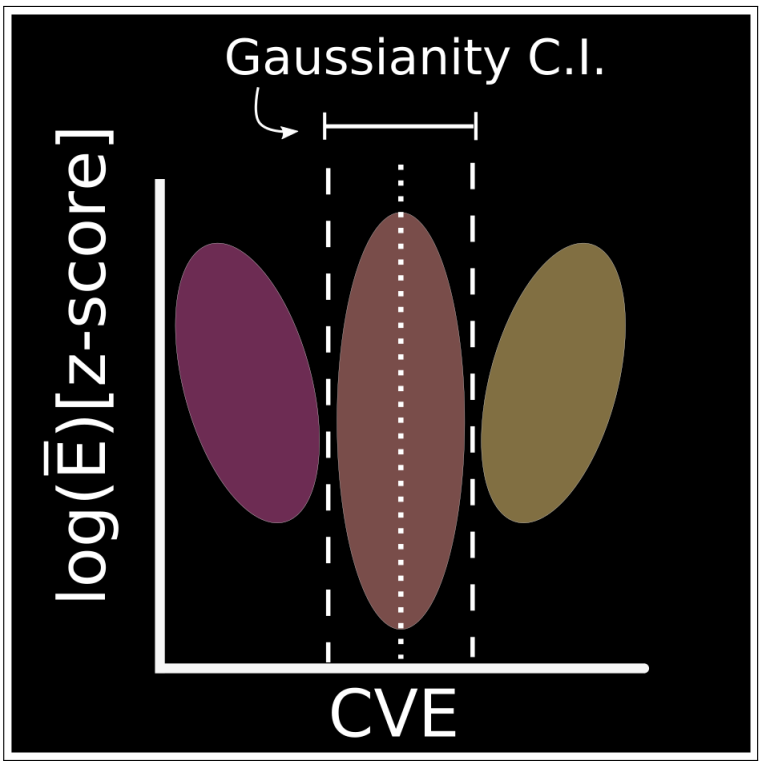

Figure 1.8: Envelope characterization space. The coefficient of variation of the envelope (CVE) and the mean of the envelope (ME) are combined in a novel 2D phase space for EEG signal classification. CVE and ME are fundamental signal parameters representing morphology and energy, respectively. ME values are log-transformed and normalized ([z-score]) to account for setup differences. The central dotted line represents the mean of the surrogate Gaussian CVE distribution, while the Gaussian CVE confidence interval (both dashed lines) defines the mid-CVE region (salmon). Consequently, the low-CVE region (purple) and the high-CVE region (gold) are also established.

1.6 Hypothesis

- The envelope analysis characterizes the human alpha rhythm as a Gaussian process, thus reflecting its absence and presence in resting-state electroencephalography recordings.

1.7 Objectives

1.7.1 General objective

- Characterize the absence and presence of the human alpha rhythm by envelope analysis.

1.7.2 Specific objectives

- Obtain resting-state human EEG recordings under eyes-open and eyes-closed conditions from open access massive databases.
- Develop source code to apply the envelope analysis to the resting-state EEG recordings.
- Apply the envelope analysis to the resting-state EEG recordings.

MATERIALS AND METHODS

2.1 Data

2.1.1 EEG data

The rs-EEG recordings from the *Leipzig study for mind-body-emotion interactions* (LEMON) dataset (Babayan et al., 2019) were used to study the human alpha rhythm signal at the scalp level. This is a cross-sectional, multi-measure dataset collected in the Max Planck Institute ecosystem and published in *Scientific data*(https://www.nature.com/sdata/), an open-access, peer-reviewed journal published by the Nature Publishing Group. The study protocol was in accordance with the declaration of Helsinki(Association et al., 2001). All subjects provided written consent prior to assessments and were screened and excluded for drug use, cardiovascular, neurological and psychiatric conditions.

rs-EEG recordings from 216 subjects were obtained in an electrically shielded and sound-attenuated room using 62 active electrodes: 1 electrooculography channel and 61 EEG channels following the 10-10 system (Oostenveld and Praamstra, 2001). The FCz electrode was established as the reference channel and the ground was

attached to the sternum. The amplitude resolution was set to 0.1 [μV] and electrode impedance was kept under 5 [kΩ]. The signals were recorded using an antialiasing bandpass filter between 0.015[Hz] and 1[kHz] and digitized at 2500 samples per second. Each subject's continuous recording included 16 60[s] blocks, 8 EO blocks and 8 EC blocks. These 16 blocks were interleaved and recordings started with the EC condition. The subjects were seated in front of a computer screen to receive directions for opening and closing their eyes.

Data from 13 participants was excluded due to low data quality and defective metadata. Recordings from the remaining 203 subjects was preprocessed as follows. The data was decimated from 2500[Hz] to 250[Hz] and bandpass filtered between 1-45[Hz] with a 8th order Butterworth filter. The recordings were split into EO and EC conditions for further processing. Outlier channels were rejected and time intervals with extreme deflection or frequency bursts were removed by visual inspection.

From the preprocessed data, the recordings from two individuals were discarded as spurious interval removal resulted in highly discontinuous time series. The sex and age information of the remaining 201 subjects is shown in Table 2.1. Only the channels O1, Oz and O2 from each subject were used for further manipulation. Figure 2.1 shows the channel length distribution after preprocessing. Channel length was 474.825$\pm$9.296[s] for the EC condition (blue) and 469.441$\pm$13.202[s] for the EO condition (orange).

Sex	
♂	♀
145	81

Age								
20-25	25-30	30-35	35-40	55-60	60-65	65-70	70-75	75-80
79	61	13	1	4	18	25	21	4

Table 2.1: Demographic information of the 201 subjects included in the analysis.

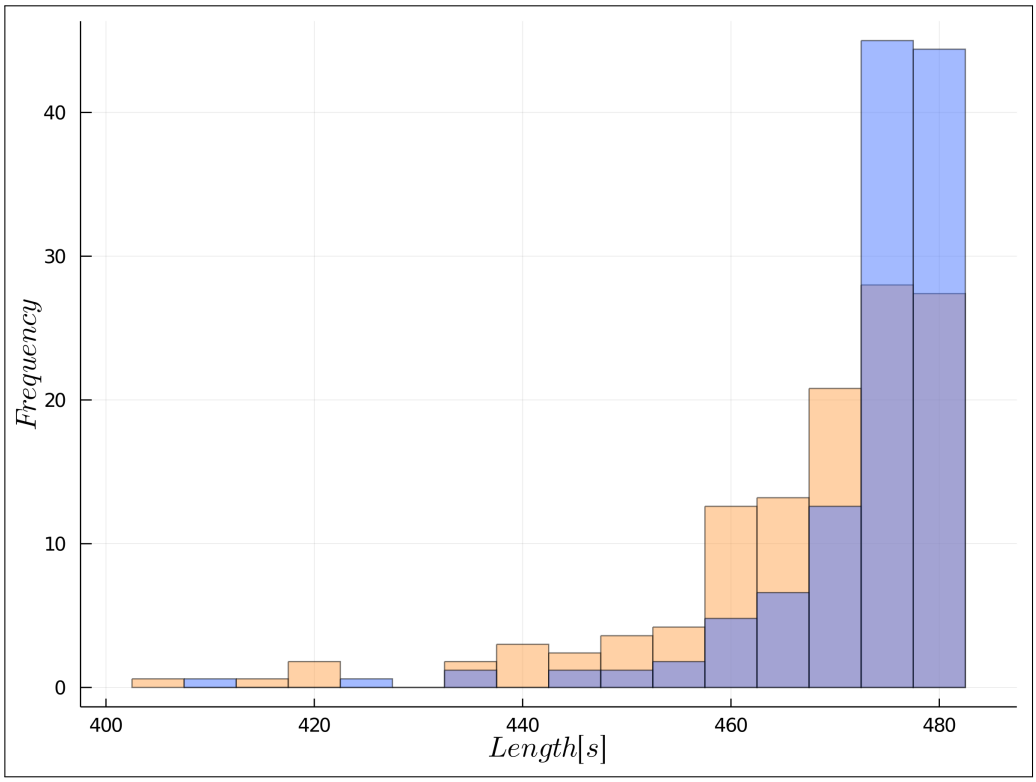

Figure 2.1: Recording length after spurious interval removal. Channel length was 474.825±9.296[s] for the EC condition (blue) and 469.441±13.202[s] for the EO condition (orange).

2.1.2 Synthetic EEG data from a population of weakly coupled oscillators

As Díaz et al. (2007) reported that the CVE characterized every behavior in the MMS model, three synthetic EEG signals were created based on signals emerging from this model. An instance of the model was simulated following Matthews et al. (1991, Section 3, Numerical results). Simulations were implemented using the DifferentialEquations.jl package (Rackauckas and Nie, 2017). A system of 800 oscillators was simulated, where natural frequencies followed a uniform distribution with bandwidth $\Delta = 0.8$. These frequencies were calculated as stated in (Matthews et al., 1991, Table 1). A 72 [s] solution was obtained numerically by a fourth-order Runge-Kutta method (Butcher, 1996) with a timestep of 1/250 for three different coupling constant K values: 1.1 (phase-locking), 0.1 (incoherence), and 0.90(chaos/unsteady state). A single 24[s] epoch for each case was selected, and to these epochs white Gaussian noise and 1/f noise(pink noise) was added to artificially introduce the classic EEG spectrum background. 6000 values were sampled from $\mathcal{N}(0, 0.05)$ to create zero mean WGN epochs with the same epoch length and sampling frequency as the experimental data. A WGN epoch was added to each simulated epoch to add a flat spectral component to the synthetic data. Similarly, pink noise was obtained filtering a WGN epoch using the filter design reported by (Corsini and Saletti, 1988), effectively introducing a 1/f spectral component in the frequency band of interest.

2.1.3 iEEG data

Besides the EEG data, an iEEG dataset was also analyzed to further study the human alpha rhythm generator dynamics. The *atlas of the normal intracranial electroencephalogram* (AN-iEEG) dataset (Frauscher et al., 2018) is a massive *resting-state intracranial electroencephalography* (rs-iEEG) dataset collected from subjects who underwent evaluation for epilepsy surgery at three different locations: Montreal Neurological Institute and Hospital, Centre Hospitalier de l'Université de Montréal, and Grenoble-Alpes University Hospital. The AN-iEEG dataset was published in *Brain: A Journal of Neurology* (https://academic.oup.com/brain), a peer-reviewed journal published by Oxford University Press.

iEEG signals were recorded while subjects remained awake and resting with their eyes closed. As the data comes from epileptic patients, iEEG channels were selected under several inclusion criteria to exclude epileptic activity. Stereotactic EEG and subdural strips and grids were used to acquire the recordings at the different locations. MRI was used to reference all electrodes locations to the ICBM152 model; a unified framework for brain mapping (Fonov et al., 2011; Mazziotta et al., 2001). 60[s] sections were visually selected from each subject individual recordings. The signals were filtered at 0.5-80[Hz] using a *finite impulse response* (FIR) filter and were downsampled to 200[Hz](unless that was the original sampling frequency). Power-line noise was reduced using an adaptive filter. From this dataset, only signals tagged as coming from occipital regions were used in the analysis. The following tags were

included: superior and middle occipital gyri; inferior occipital gyrus and occipital pole; cuneus; calcarine cortex; lingual gyrus and occipital fusiform gyrus.

2.2 EEG envelope analysis

The pipeline reported by Díaz et al. (2018) was applied to the rs-EEG data. All procedures were implemented using the Julia programming language (Bezanson et al., 2017) (https://julialang.org). The pipeline is shown in Figure 2.1.

Filtering and epoching

The data was filtered in the alpha band using a zero phase *infinite impulse response* (IIR) filter, in particular a 2nd order bidirectional Butterworth filter. This type of filter introduces zero delay in the time domain to each frequency component, and thus contributes to conserve the signal waveform. It is implemented by two successive applications of filtering and reversion of the original signal (Kormylo and Jain, 1974). The filter's impulse response and step response are shown in Figure 2.3. Similarly, a Bode plot is presented in Figure 2.4 to visualize its frequency response. Given that the phase response is constant and zero, only the magnitude response is shown. Each channel was divided into 24[s] epochs (6000 points per epoch) with an overlap of 50%. This amounts to 22893 epochs for the EC condition and 22634 for the EO condition.

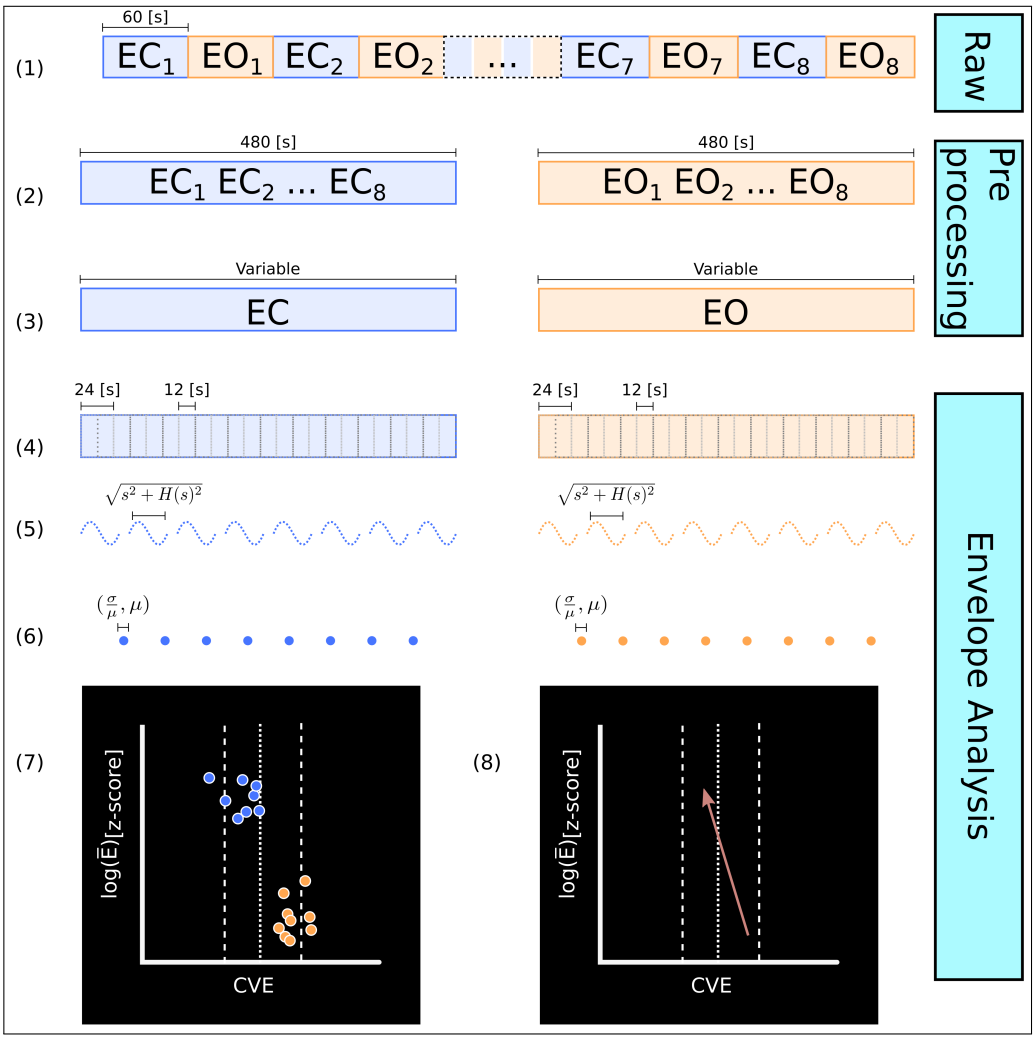

Figure 2.2: Pipeline applied to LEMON dataset EEG recordings. **(1)** Raw signal. 16 blocks of 60 seconds, 8 eyes-closed blocks and 8 eyes-open blocks, were recorded at 2500 [Hz]. The blocks were interleaved and the recording started with eyes closed. **(2)** Concatenation of eyes-closed and eyes-open blocks. The resultant signals were downsampled to 250[Hz] and bandpass-filtered between 1-45[Hz] with a 8th order Butterworth filter.**(3)** Spurious time intervals were removed by visual inspection. PCA and ICA was applied for further artifact removal.**(4)** Only O1, Oz, and O2 channels were using for further manipulation. The alpha band (8-13[Hz]) was isolated by bidirectional filtering using a 2nd order Butterworth filter. The data was divided in 24[s] epochs with an overlap of 12[s]. **(5)** The envelope ($env = \sqrt{s^2 + H[s]^2}$) was calculated from these 24[s] epochs. 2[s] segments were excised from both tails, resulting in 20[s] envelopes. **(6)** The coefficient of variation of the envelope (CVE) and the mean of the envelope (ME) were estimated. **(7)** The envelope characterization space (EnvSpace) was constructed using (CVE,ME) values from all subjects. The logarithm of the ME values were calculated and normalized with reference to each subject, each channel mean and standard deviation. **(8)** The centroid of the (CVE,$log(ME)[z-score]$) cloud was estimated for each subject, each channel data for both conditions. A single vector was traced from the eyes-open centroid to the eyes-closed centroid as a measure of overall change between conditions in the EnvSpace.

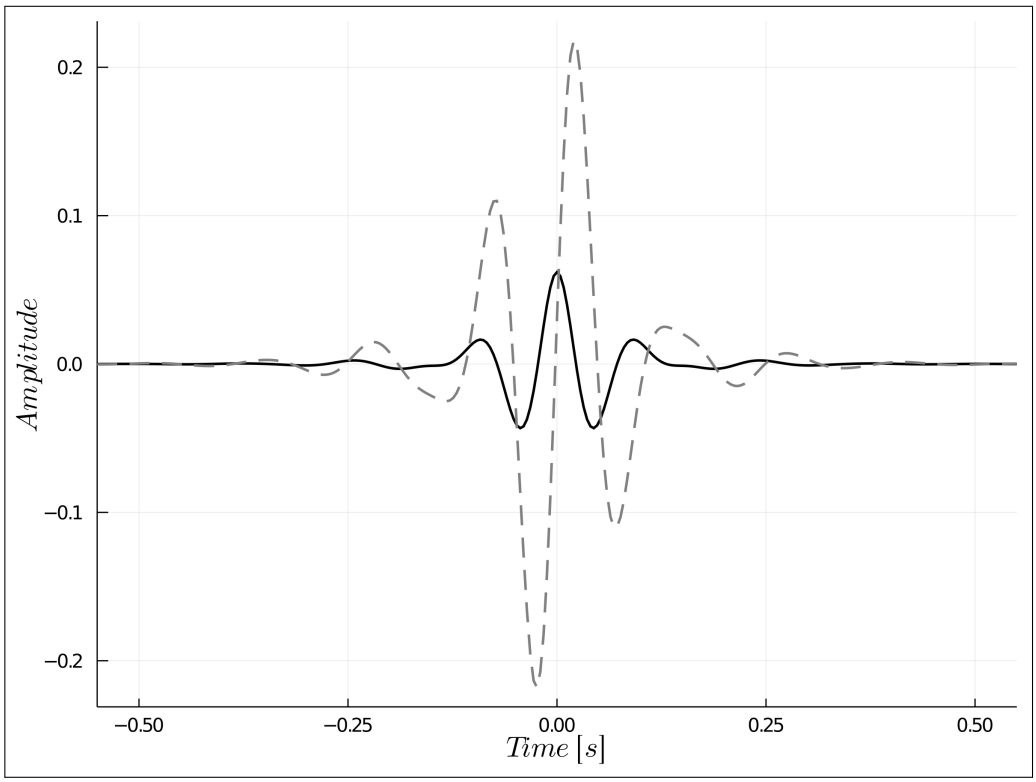

Figure 2.3: Filter time response. The impulse response (black solid trace) and the step response (gray dashed trace) of the bidirectional 2nd order Butterworth filter.

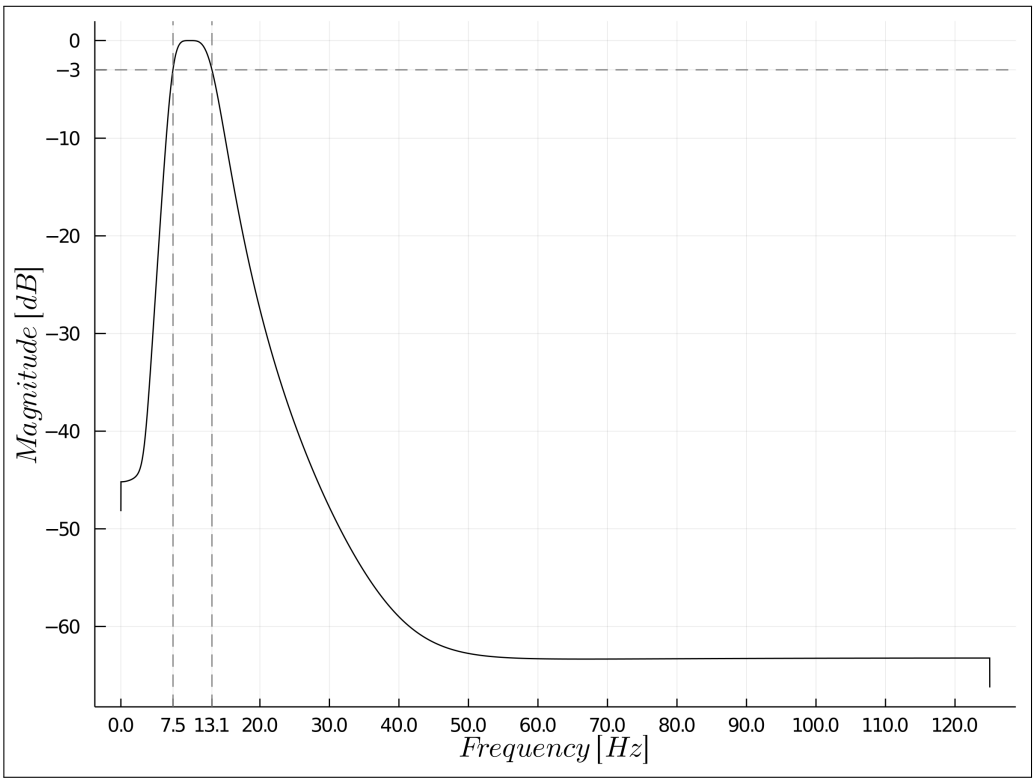

Figure 2.4: Filter frequency response. The magnitude response shows that the -3dB cutoff frequencies are 7.5 and 13.1. The phase response is constant and zero, and thus is not shown.

Envelope parameters estimation

The analytic signal was computed for each epoch as in Equation 1.13 and its envelope was obtained using Equation 1.18. 2[s] segments were excised from each tail of the estimated envelope to correct for spurious effects due to both filtering and analytic signal computation. From these 20[s] envelopes, the coefficient of variation of the envelope was calculated as in Equation 1.19, as well as the mean of the envelope.

Gaussian CVE probabilistic model, CVE classes, and experimental CVE distributions

To obtain the PDF for the CVE of discrete WGN. 10^6 instances of a 6000 points epoch were simulated, with each point sampled from a normal standard distribution $\mathcal{N}(0, 1)$. The number of points was set to match the experimental data epoch length and sampling frequency. These *in silico* generated epochs were processed as described for the experimental data. The same filter was applied to filter the WGN epochs in the alpha band. The envelope was calculated, 2[s] segments were cut from both ends, and the CVE and ME values were computed. Then, the PDF for the CVE values of these alpha-filtered zero mean WGN epochs was calculated. The 0.005 and 0.995 quantiles were estimated to obtain the lower and upper limits of a 99% confidence interval to assess the null hypothesis $H_0 : CVE_{epoch} = CVE_{Gaussian}$. Thus, the three CVE classes were established as: $CVE < 0.5\%$(low CVE), $0.5\% \leq CVE \leq 99.5\%$(mid CVE), and $99.5\% < CVE$(high CVE). For clarity, these CVE classes were color-coded following the buda color scheme (Crameri, 2018) as purple (low-CVE), salmon (mid-CVE), and gold (high-CVE). The CVE distribution and the percentage of values lying in each CVE class were calculated for both experimental conditions. The experimental conditions were also color-coded as blue for EC data and orange for EO data.

Envelope characterization space: scatterplots, density maps, and vector fields

To construct the EnvSpace, the ME values for each subject, each channel data were log-transformed and normalized (represented as $[z - score]$) using each channel's mean and standard deviation. The resultant bivariate $(CVE, log(ME)[z - score])$ time series for both experimental conditions were plotted in the envelope characterization space as scatterplots. The alpha channel was set to 50% to highlight cluster density. Additionally, 2D histograms were constructed using a 500x500 matrix. The rows and columns of these 2 matrices were filtered using a 51-coefficient binomial kernel. The resultant matrices were visualized using an alternating color-white palette to obtain a contour-like plot of the 2D histograms. Also, the overall change between conditions was examined computing the EC centroid and the EO centroid for each subject, each channel data. A single vector was traced from the EO centroid to the EC centroid, and these were depicted as a white dot and as the arrow head, respectively. Vectors were classified depending on the value of the EC centroid CVE coordinate and were color-coded following the CVE class color code (alpha channel was set to 50%), creating a vector field inside the EnvSpace where channels were classified depending on their overall CVE behavior.

Experimental condition, spectrogram and CVEgram.

Time-frequency analysis was applied to a 960[s] channel (no interval removal) to compare the time-varying spectral profile of the human alpha rhythm with its CVE fluctuations. The EO and EC data was first reconcatenated to recover the original interleaved protocol. Then, the data was segmented in 20[s] epochs with 50% of overlap and processed according to Prerau et al. (2017) to produce a multitaper spectrogram. The time-bandwidth value was set to 10[s] and 20 tapers were used, defining a frequency resolution of 0.5[Hz]. Only frequencies in the interval [1,20] were kept and spectral power was log-transformed and color-coded (dark blue $<$ cyan $<$ yellow $<$ dark red). The multitaper spectrogram was set into a common temporal reference together with the temporal CVE fluctuations and the changes in experimental condition to visualize the correlation between these three variables.

Fourier analysis/EEG envelope analysis comparison

One raw representative epoch from each CVE class during the EC condition was selected for re-analysis using both Fourier analysis and EEG envelope analysis. Before filtering, the spectral profile of each epoch was computed. After filtering, the envelope, CVE and ME were calculated for these three alpha-filtered experimental epochs. ME values were log-transformed and normalized to re-obtain the EnvSpace. The resultant spectral profiles and (CVE,log(ME)[z-score]) points were color-coded based on CVE class and visualized along with the alpha-filtered epochs (and their re-

spective envelopes) for comparison. The same procedure was applied to the synthetic EEG signals coming from a population of weakly coupled nonlinear oscillators.

2.3 iEEG envelope analysis

To implement the *iEEG envelope analysis* (EnviEEG), rs-iEEG data was treated identically to the rs-EEG, with some exceptions. The Gaussian CVE probabilistic model was recalculated using a sampling frequency equal to 200[Hz] to match the AN-iEEG sampling frequency. Filtering, epoching, and envelope parameters estimation remained untouched. Overall, 416 rs-iEEG epochs were analyzed. While constructing the EnvSpace, ME values were log-transformed but not normalized as AN-iEEG contains EC data only. To compare Fourier analysis with iEEG envelope analysis, three representative epochs recorded from the calcarine cortex were selected and re-analyzed using both methods.

RESULTS

3.1 EEG envelope analysis

3.1.1 Surrogate and experimental CVE distributions

The experimental CVE distributions for both conditions are shown in Figure 3.1 (black traces), along with the surrogate Gaussian CVE distribution (gray traces, both panels). The 99% confidence interval for Gaussianity is [0.460,0.586], meaning that any epoch whose CVE lies inside this interval is considered to be indistinguishable from white Gaussian noise. Most epochs in the eyes-closed CVE distribution display either a mid-CVE or a high-CVE profile (44.33% and 46.1%, respectively), showing that Gaussian and phasic epochs predominate in the alpha-filtered occipital recordings of the LEMON dataset subjects when they rest with their eyes closed. There is also a substantial contribution of low-CVE, rhythmic signals (9.56%). On the contrary, the low-CVE contribution to the eyes-open CVE distribution is negligible (0.56%, as expected from pure noise), while most epochs lie in the mid-CVE (55.59%) and high-CVE (43.85%) regions.

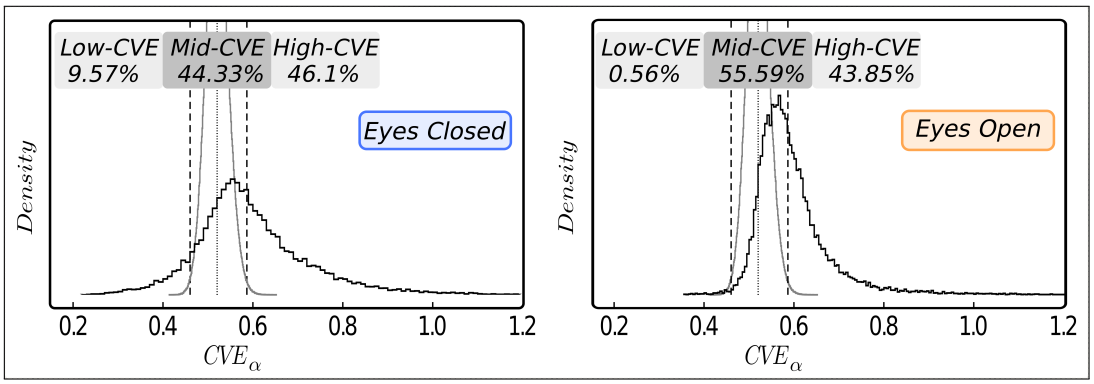

Figure 3.1: CVE distributions for surrogate and experimental EEG data. The surrogate Gaussian CVE distribution (gray traces, both panels) is bell-like and narrow around its mean value 0.520(dotted line); as expected close to $\sqrt{(4-\pi)/\pi}$. The lower and upper limit of the 99% confidence interval for Gaussianity (dashed lines) are 0.460 and 0.586, respectively. For EC epochs (blue), 44.33% are in the Gaussian class, while 9.57% and 46.1% present low and high CVE values, respectively. For EO epochs(orange), 55.59% are Gaussian, 43.85% show high CVE values, and only 0.56% present low CVE values.

3.1.2 Envelope characterization space: scatterplots, density maps, and vector fields

The scatterplot between the CVE and the ME values of alpha-filtered epochs in both experimental conditions is shown in Figure 3.2. The eyes-closed data(blue) presents low energy epochs that are mostly associated with Gaussian CVE values and show energy values similar to the eyes-open data (orange). On the other hand, high energy epochs are found in all three CVE classes. Low-CVE epochs cluster around 1 standard deviation above the mean, while high-CVE epochs show a broader distribution in the high energy region. Similarly, Gaussian CVE epochs lie across the high energy region, and they reach the highest energy profile in the EC data. On

the contrary, mid-CVE epochs in the EO data are mostly found in the lower energy zone, together with high-CVE epochs as well. Low-CVE epochs are almost absent during the EO condition.

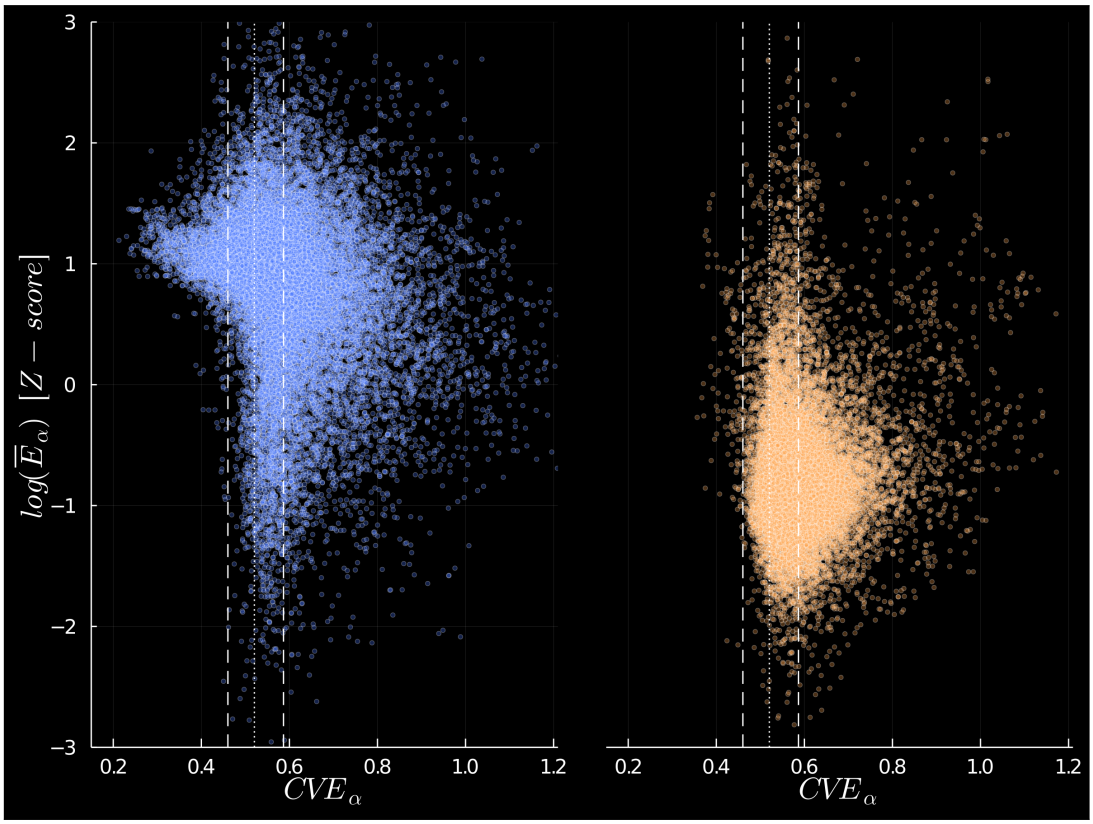

Figure 3.2: EEG envelope characterization space scatterplots. CVE values and ME values (log-transformed and normalized) for eyes-closed(blue) and eyes-open (orange) data are visualized in the envelope characterization space. Low energy EC data is mostly contained in the Gaussian region, but high energy epochs are associated with all three CVE classes. EC low-CVE epochs group around 1 standard deviation above the mean, while high energy mid-CVE and high-CVE epochs are more broadly distributed. Most EO epochs are low energy epochs associated with either mid-CVE and high-CVE values. Dashed lines represent the 99% confidence interval for Gaussianity, while the dotted line marks the mean of the surrogate Gaussian CVE distribution. Marker alpha channel was set to 50% to highlight cluster density.

The density map in Figure 3.3 reveals the underlying clustering pattern of the experimental data in EnvSpace. The experimental joint distributions of $(CVE, log(ME)[z-$

score]) values for both conditions were smoothed using a binomial kernel to obtain a contour-like visualization. The experimental bivariate distributions are unimodal during both conditions. While EC data clearly clusters around the Gaussian region, 1 standard deviation above the mean energy, EO data also group around the mid-CVE region but 1 standard deviation below the mean energy.

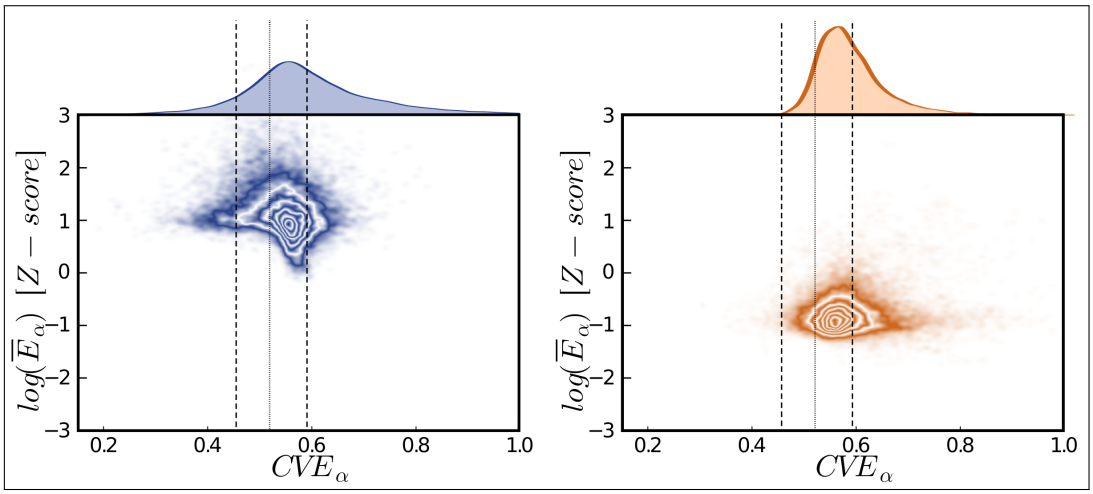

Figure 3.3: EEG envelope characterization space density maps. The joint probability distributions of $(CVE, log(ME)[z-score])$ values for eyes-closed (blue) and eyes-open(orange) are both unimodal and centered around the Gaussian region. While both Gaussian, the EC centroid is located 1 standard deviation above the mean energy, and the EO centroid is located 1 standard deviation below the mean energy. Dashed lines represent the 99% confidence interval for Gaussianity, while the dotted line marks the mean of the surrogate Gaussian CVE distribution. Distributions were plotted using a color-white palette to obtain a contour-like visualization.

The analysis of each subject, each channel data mirrors the results found for the entire population at the individual channel level. Vectors were traced from the EO centroid to the EC centroid of each channel time series in the EnvSpace and classified by their EC centroid CVE coordinate (Figure 3.4). Thus, these vectors represent the overall change in EnvSpace from the EO to the EC condition. The amount of

vectors in each CVE class roughly resembles the EC CVE distribution, while most EO centroids display either a mid-CVE or high-CVE profile. The presence of low-CVE channels reveals that some recordings are intrinsically rhythmic and that the $\approx 10\%$ of low-CVE epochs during the EC condition is not simply due to marginal accumulation during Gaussian and high-CVE processes. Remarkably, most vectors show a overall change in energy of about 2 standard deviations regardless of the CVE values involved. This energy change between conditions at the single channel level resembles the result obtained at the population level (density maps, Figure 3.3).

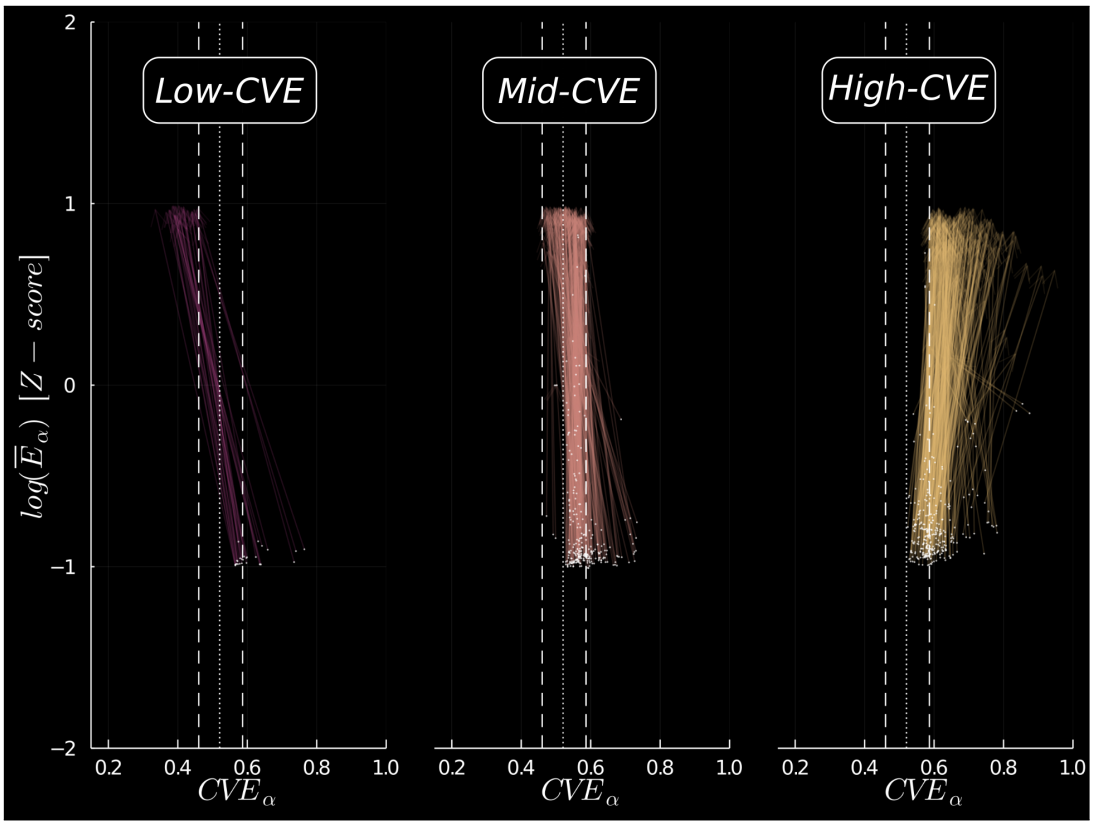

Figure 3.4: EEG envelope characterization space vector fields. Vectors were traced from the EO centroid (white dot) to the EC centroid (arrowhead) of each channel data. Each vector was classified according to its EC centroid CVE coordinate. While EO centriods are confined to the mid-CVE and high-CVE regions, EC centroids are distributed in all CVE classes. Noticeably, most vectors show an overall change in energy of about 2 standard deviations regardless of the CVE values involved. Dashed lines represent the 99% confidence interval for Gaussianity, while the dotted line marks the mean of the surrogate Gaussian CVE distribution. Alpha channel was set to 50% to highlight cluster density.

3.1.3 Relation between experimental condition, spectrogram, and CVE

A closer look into the time-varying behavior of spectrum and CVE further supports that a increase in alpha energy correlates with all different CVE classes. A single

recording (channel O1) that suffered no interval removal during the preprocessing stage and whose eyes-closed centroid lies in the high-CVE region was explored setting the behavioral condition, spectra, and CVE into a common temporal frame (Figure 3.5, left panel). While epochs of all CVE classes are found during this 960[s] continuous recording. Regardless of their particular CVE, all epochs show an increased alpha power during the EC blocks. Epochs in the edge between behavioral conditions show a very high CVE value, but this is to be dismissed as an artifact because these epochs contain data from both conditions, thus appearing pulsating. Three representative EC epochs are marked with their respective CVE color code in the CVEgram, and they are shown together with their CVE for further inspection (Figure 3.5, right panel). Maximum amplitude is 30-40[μV] for all epochs. While the Gaussian epoch shows a CVE close to $\sqrt{(4-\pi)/\pi}$, the non-Gaussian epochs present CVE values far away from the limits of the 99% confidence interval for Gaussianity. Accordingly, it can be seen that the low-CVE epoch is distinctively rhythmic, and the high-CVE epoch is obviously pulsating, as expected.

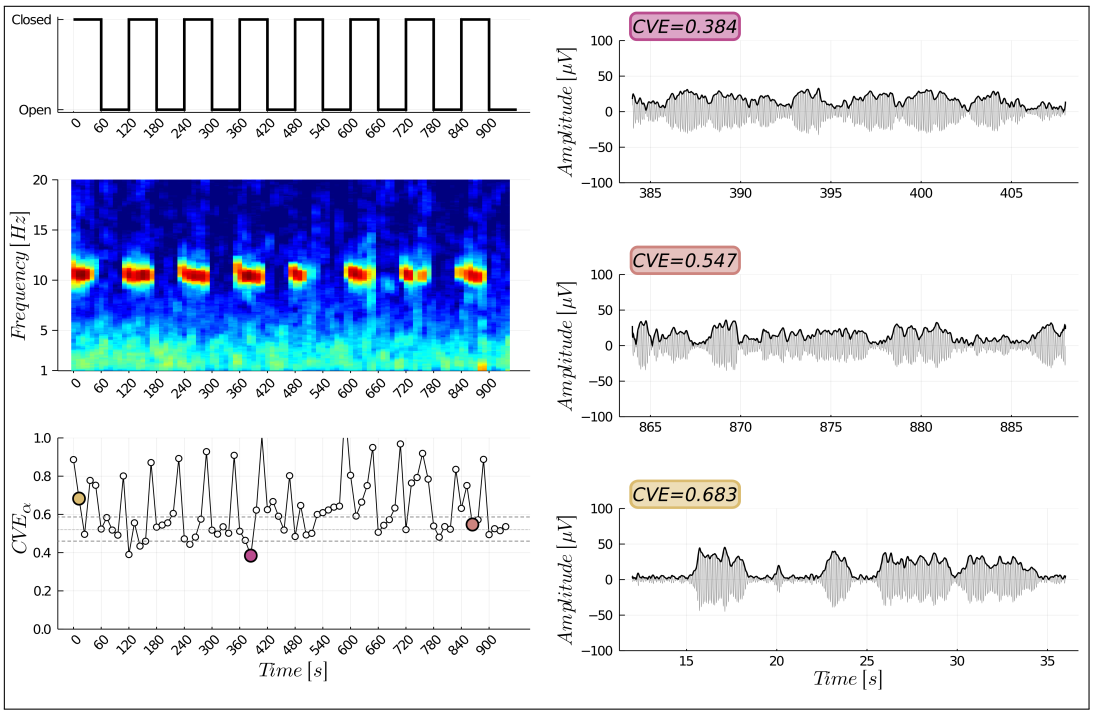

Figure 3.5: Temporal covariation between experimental condition, spectrogram, and CVE. Left panel, from top to bottom: experimental condition, multitaper spectrogram, and CVEgram of 960[s] continuous recording. All EC blocks correlate with an increase in alpha band energy regardless of their CVE value. Three representative epochs (one for each CVE class) are marked in the CVEgram and plotted together with their respective CVE (right panel). The Gaussian epoch shows a CVE close to $\sqrt{(4-\pi)/\pi}$, while the low-CVE and the high-CVE epochs are distinctively rhythmic and pulsating, respectively. Dashed lines represent the 99% confidence interval for Gaussianity, while the dotted line marks the mean of the surrogate Gaussian CVE distribution.

3.1.4 Fourier analysis/EEG envelope analysis comparison

The human alpha rhythm has been historically identified by its spectral profile, while a similar spectrum has also been found in phase-locking signals emerging from populations of weakly coupled oscillators. Thus, it seems appropriate to compare the spectral and CVE profiles of synthetic alpha-like signals (Figure 3.6) and experimen-

tal eyes-closed rs-EEG recordings (Figure 3.7). A population of 800 MMS model oscillators was simulated to obtain signals from three different regimes: phase-locking, incoherence, and chaos. Also, white noise and pink noise was added to artificially introduce the classic EEG spectral background. The synthetic EEG signals were alpha-filtered and classified according to their CVE (Figure 3.6.a). While these three epochs present different CVE values, their pre-filtering spectra (Figure 3.6.b) are very similar, although the phase-locking signal presents the highest and the incoherence signal the lowest energy at ≈ 10[Hz]. In the EnvSpace (Figure 3.6.c), the three synthetic epochs can be easily distinguished by their CVE. Similarly, three experimental alpha-filtered epochs (same epochs in Figure 3.5) are shown in Figure 3.7.a . The pre-filtering spectra (Figure 3.7.b) are almost indistinguishable from each other, and the canonical peak at ≈ 10[Hz] is much broader than the synthetic one (Figure 3.6.b). While the spectral profile cannot discriminate between these epochs alone, they can be clearly distinguished by their CVE values in the EnvSpace(Figure 3.7.c).

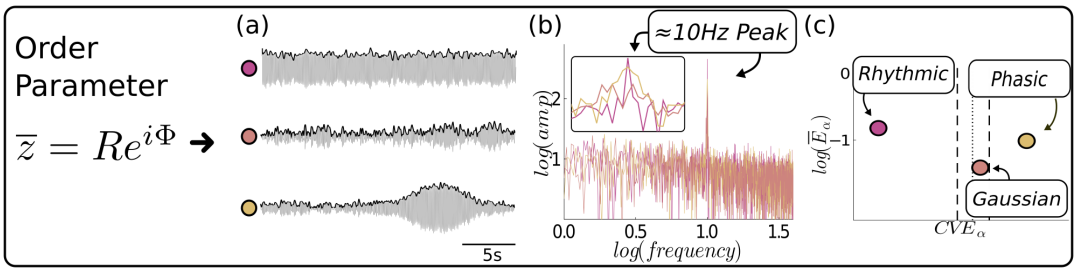

Figure 3.6: Fourier/EnvEEG comparison for synthetic EEG signals. Three synthetic EEG epochs (one for each CVE class) coming from a population of weakly coupled nonlinear oscillators were analyzed by Fourier analysis and EEG envelope analysis. **(a)** The three alpha-filtered epochs (and their respective envelopes in black) show the expected signal morphology. **(b)** All epochs contain high energy at $\approx$ 10[Hz] and their spectra are very similar, even though the low-CVE epochs contains the highest energy and the mid-CVE the lowest. **(c)** The epochs can be clearly distinguished by their CVE in the envelope characterization space. Dashed lines represent the 99% confidence interval for Gaussianity, while the dotted line marks the mean of the surrogate Gaussian CVE distribution.

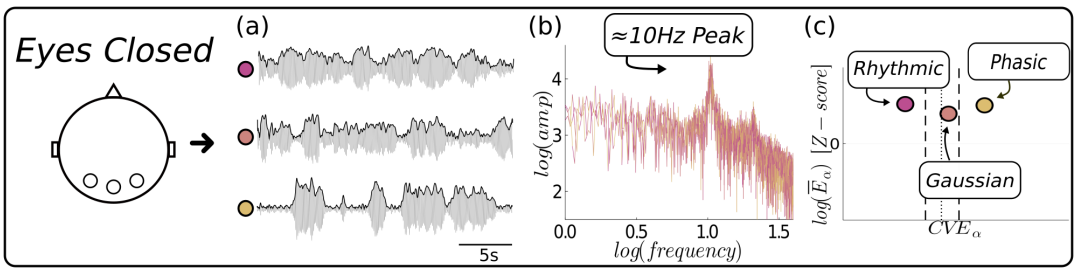

Figure 3.7: Fourier/EnvEEG comparison for experimental EEG signals. Three experimental eyes-closed EEG epochs (one for each CVE class, same epochs displayed in Figure 3.5) coming from a O1 channel were analyzed by Fourier analysis and EEG envelope analysis. **(a)** The three alpha-filtered epochs (and their respective envelopes in black) show the expected signal morphology. **(b)** While all epochs contain high energy at $\approx$ 10[Hz], their spectra are almost indistinguishable from each other. **(c)** The epochs can be clearly distinguished by their CVE in the envelope characterization space. Dashed lines represent the 99% confidence interval for Gaussianity, while the dotted line marks the mean of the surrogate Gaussian CVE distribution.

3.2 iEEG envelope analysis

3.2.1 Surrogate CVE distribution

The surrogate Gaussian CVE distribution for the AN-iEEG data was estimated using the same epoch length and filter applied to the LEMON data, but matching the AN-iEEG sampling frequency. The resultant 99% confidence interval for Gaussianity is [0.460,0.587], while the mean of the surrogate Gaussian CVE distribution is 0.520.

3.2.2 Envelope characterization space: scatterplots

Data from all iEEG occipital recordings is visualized in the EnvSpace (Figure 3.8, left panel). Most epochs are Gaussian, while a small percentage lies in both non-Gaussian regions. Energy values were not normalized because the AN-iEEG data contains EC data only. Thus, relative differences in epoch energy among subjects are not evident here. Additionally, as iEEG data has been shown to vary between recordings millimeters apart (Cooper et al., 1965), rs-iEEG data coming from the calcarine cortex was analyzed independently (Figure 3.9, right panel). The calcarine cortex is of special importance as the purest alpha rhythm signals have been reported to come from this structure in dogs (Lopes da Silva et al., 1973). Calcarine cortex epochs are also clearly grouped in the Gaussian region, and the amount of non-Gaussian epochs is negligible.

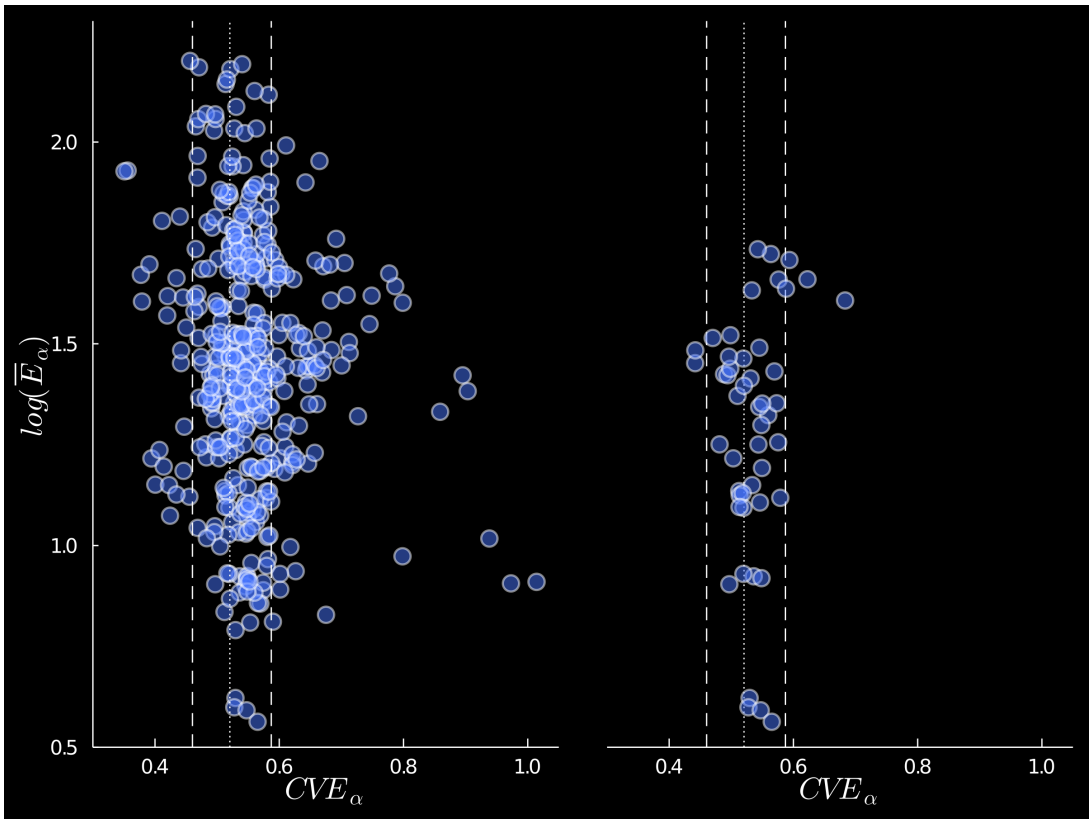

Figure 3.8: iEEG envelope characterization space scatterplots. CVE values and ME values (log-transformed) for all occipital recordings (left panel) group mainly in the Gaussian region, while a small amount is distributed in both non-Gaussian regions. Notice that ME values were not normalized, and thus relative difference in energy is not evident here. Calcarine cortex data is shown independently (right panel). Most epochs are Gaussian. Non-Gaussian epochs are almost absent. Dashed lines represent the 99% confidence interval for Gaussianity, while the dotted line marks the mean of the surrogate Gaussian CVE distribution. Marker alpha channel was set to 50% to highlight cluster density.

3.2.3 Fourier analysis/iEEG envelope analysis comparison

Three representative rs-iEEG epochs recorded at the calcarine cortex were analyzed using both Fourier and EnviEEG (Figure 3.9). The three alpha-filtered epochs (one for each CVE class) are shown in Figure 3.9.a, while their pre-filtering spectra are depicted in Figure 3.9.b. These spectra are almost identical; the same trend was

observed in the synthetic and experimental EEG data (Figure 3.6 and Figure 3.7). Nonetheless, the spectral peak in the alpha band seems to be much broader than the EEG spectral counterpart. Again, these three experimental epochs are easily recognized in the EnvSpace by their CVE (Figure 3.9.c). Notice that epochs come from different subjects, and thus the difference in energy is not comparable.

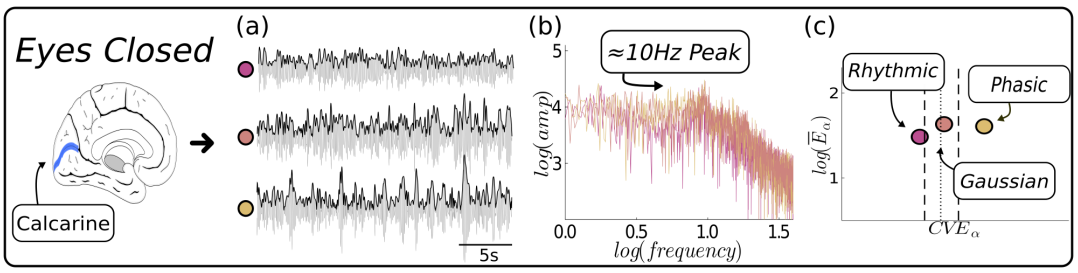

Figure 3.9: Fourier/EnviEEG comparison for experimental iEEG signals. Three experimental eyes-closed iEEG epochs(one for each CVE class) coming from the calcarine cortex were analyzed by Fourier analysis and iEEG envelope analysis. **(a)** The three alpha-filtered epochs (and their respective envelopes in black) show the expected signal morphology. **(b)** Their spectra are almost indistinguishable from each other. While all epochs contain high energy at $\approx$ 10[Hz], the spectral peak is much broader than the EEG counterpart. **(c)** The epochs can be clearly distinguished by their CVE in the envelope characterization space. Dashed lines represent the 99% confidence interval for Gaussianity, while the dotted line marks the mean of the surrogate Gaussian CVE distribution.

DISCUSSION

This work aimed to characterize the human alpha rhythm using a novel signal analysis method: the envelope analysis. This method relies on the study of coefficient of variation of the envelope to detect both Gaussian and synchronous processes. The main motivation behind this endeavor was, on the one hand, the extensive literature around the topic of neural synchronization, and how this concept was created at the very cradle of the EEG field by Lord Adrian while studying the human alpha rhythm. On the other hand, there is also a group, albeit sometimes dismissed, of researchers that dared to go against the stream and advocated for the recognition of Gaussian EEG phenomena, thus pointing out the resemblance between Gaussian noise and the alpha rhythm. Interestingly, this perspective also emerged early in the field with the work of renowned Japanese scientist Dr. Koiti Motokawa. Somehow, Gaussianity detection in time series has had its ups and downs, never reaching a decisive point, and thus Adrian's and Motokawa's approaches have never encountered a firm reference point for further discussion. In order to contribute to the final elucidation of this debate, I studied the human alpha rhythm using the envelope analysis.

Some points about the method require a closer observation. While the origin of the EnvEEG can be traced back to Motokawa's report on the Rayleigh distribution in EEG data (Motokawa, 1943; Rao and Edwards, 2008), it was Dick and Vaughn (1970) who realized that the study of the time-varying behavior of the human alpha rhythm envelope could be used to assess Gaussianity. They proposed to segment the filtered signal to follow the changes of the variance or standard deviation of the envelope over time. Thus, EnvEEG relies on this segmentation strategy to approximate a stationary process. This segmentation strategy, however, is not free from drawbacks. In general, it is not know how long EEG stationary epochs are as this feature changes between experimental conditions Barlow (1985). While the epoch length used in this work may not be completely appropriate, the results of Díaz et al. (2018) in rat EEG are reassuring as CVE displayed a high degree of constancy in different behavioral conditions. Also, visual inspection of alpha rhythm epochs showed that they are very stable over the period selected. Another crucial point is that the surrogate Gaussian CVE distribution necessary to apply the EnvEEG depends on both epoch length and bandwidth (as well as sampling frequency), shorter epochs and narrower bandwidths producing a higher variance in this distribution. Therefore, CVE Gaussianity detection in itself involves uncertainty about where in the time-frequency domain Gaussianity is taking place. This is, of course, expected as the same scenario is well-known in Fourier analysis and its applications (Folland and Sitaram, 1997). EEG Gaussianity reports have advanced divergent results precisely because they have used different combinations of epoch length and sampling

frequency (McEwen and Anderson, 1975), while different bandwidth effects are hard to assess as filter characteristics are seldom reported. Previous studies have in fact reported Gaussianity in alpha rhythm signals using different combinations of these three parameters (Dick and Vaughn, 1970; Saunders, 1963). While this diversity does not necessarily invalidate their claims, it is important to keep these subtleties in mind when comparing their results with the results of this work.

As the LEMON dataset contains rs-EEG recordings of over 200 subjects, it is particularly helpful to explore inter-individual differences in human alpha rhythm signals. Strong differences in alpha rhythm amplitude modulation patterns among subjects is a fact both early recognized and surprisingly ignored in the EEG literature. Although this may seem a small detail, it is of fundamental importance as Gaussian and synchronous regimes display distinct amplitude modulation patterns — a feature that is captured and quantified by the CVE. Accordingly, the human alpha rhythm was shown to be sometimes a Gaussian or a synchronous signal by its CVE hallmark. Furthermore, different recordings showed a marked preference toward either low-CVE, mid-CVE, or high-CVE values, in clear accordance with early reports of different alpha modulation patterns and suggesting generator dynamics may be an individual trait. Remarkably, the change between eyes-open and eyes-closed conditions was not reflected as a change in CVE but was mirrored by a approximately constant change in energy regardless of the CVE values involved both at the single-channel and the population level, showing that the distinctive alpha rhythm's high energy profile can be produced by different generator dynam-

ics. Nonetheless, these claims should be taken with caution as the LEMON rs-EEG signals underwent a process of interval removal that, while minimal, may introduce spurious effects into CVE estimates. In any case, the analysis of an untouched continuous recording showed that Gaussian and synchronous dynamics may coexist at the scalp level in a single subject. More importantly, the simultaneous use of Fourier analysis and EnvEEG revealed that experimental epochs from all CVE classes contain the canonical spectral peak at ≈ 10[Hz], demonstrating that the very same result can be produced by rhythms, pulsating ripples, and Gaussian noise.

This result has important implications for the EEG field. The mainstream interpretation attributes the appearance of the alpha rhythm signal to event-related synchronization, and its disappearance when subject open their eyes to event-related desynchronization, while the envelope analysis is showing that this is not the case. This interpretation rests upon two widely accepted assumptions: (i) that only synchronous process can attain amplitudes sufficiently large to be measured at the scalp and (ii) that asynchronous process are self-destructive as randomly distributed phases tend to cancel each other, producing a zero amplitude signal. On the contrary, it is almost impossible that the phases of oscillators in an uncoupled population cancel each other as this accounts for only one from the infinite amount of phase combinations in the system. In fact, amplitude death is a well-described regime that only takes place in weakly coupled oscillators systems with relatively high coupling constants (Saxena et al., 2012). Certainly, synchronous signals do generate relatively high amplitude signals. The amplitude of a signal, however, cannot account com-

pletely for the underlying neural generator as the amount of neural elements recruited into the process can change over time (Elul, 1972). This is the reason behind the need for an scale-independent parameter such as the CVE. Hence, envelope analysis puts Gaussianity and synchronization in a single framework, opening the door for the concurrent monitoring of these two dichotomous brain dynamics in EEG signals.

The same one-to-many relation between spectrum and CVE was also observed in synthetic EEG signals coming from the Matthews–Mirollo–Strogatz model. The fact that frequency-locking Matthews–Mirollo–Strogatz model signals display the canonical spectral peak at ≈ 10[Hz] is not unexpected, as Kuramoto himself pointed out the relation between his model and the human alpha rhythm (Kuramoto, 1975). Surprisingly, this spectral profile was also present in incoherence and chaos signals; two process that differ substantial in terms of coupling constant and signal waveform. This apparent paradox can be easily explained considering the nature of the Fourier transform. The Fourier transform represents a signal as a linear sum of complex sinusoids, each Fourier component having an amplitude and a phase. Thus, the complex sinusoids that constitute the Fourier transform in all three CVE classes have a relatively high amplitude ≈ 10[Hz], but their phase profiles are different. This multiplicity of time domain features that are indistinguishable looking at the spectral profile alone has been already recognized in the neurosciences (Jones, 2016), and CVE offers an avenue for its detection and quantification.

The analysis of the AN-iEEG dataset revealed some differences when compared to the EEG data. The occipital rs-iEEG signals showed a strong clustering in the

Gaussian region, as opposed to the broader presence of low-CVE and high-CVE epochs in the occipital channels of the LEMON dataset, but it is worth noticing that for the former the sample size is much smaller. Interestingly, the data recorded from the calcarine cortex was almost purely Gaussian, raising the question about whether the large proportion of synchronous epochs detected at the scalp level were a byproduct of volume conduction. Also important is that rs-iEEG data displayed a broader spectral peak than the EC rs-EEG data, even though the skull is considered to not be a temporal filter, and thus this broader profile may reflect the purity of the signal recorded (Pfurtscheller and Cooper, 1975). In any case, the neural structure responsible for the generation of the human alpha rhythm is still not known. While it is remarkable that weakly coupled oscillators systems can generate data that resemble alpha rhythm signals both from the Fourier and envelope perspective, the actual relation between neural networks and weakly coupled oscillators systems is, however, yet to be defined (Breakspear et al., 2010).

Future studies regarding the alpha rhythm's CVE hallmark should trade scope for precision and focus on the concurrent measurement of EEG and iEEG signals from the visual cortex under resting-state conditions. Additionally, the same method could be used to characterize the filtering properties of the skull-meninges-skin system and its effects in the Fourier phase profile and CVE hallmark. Finally, the envelope analysis itself could be applied to other EEG, local field potential, and magnetoencephalography signals to better our understanding of Gaussian and synchronous dynamics in the nervous system.

CONCLUSIONS

In this thesis I took the intuition of using the coefficient of variation of the envelope of neural signals as a valuable classification parameter and applied it to human EEG (Díaz et al., 2007). Usually EEG epochs, lasting from few seconds to minutes, are only classified according to their energy spectrum (i.e. the energy content in small frequency bands). Nonetheless, the use of the coefficient of variation of the envelope opens a new dimension to analysis by incorporating the amplitude modulation profile of an epoch as an important descriptor specially when coupled with its energy. Thus, I have extended the analysis presented by Díaz et al. (2018) in the rat to human EEG and have shown how the envelope characterization space can effectively be used to interpret human EEG.

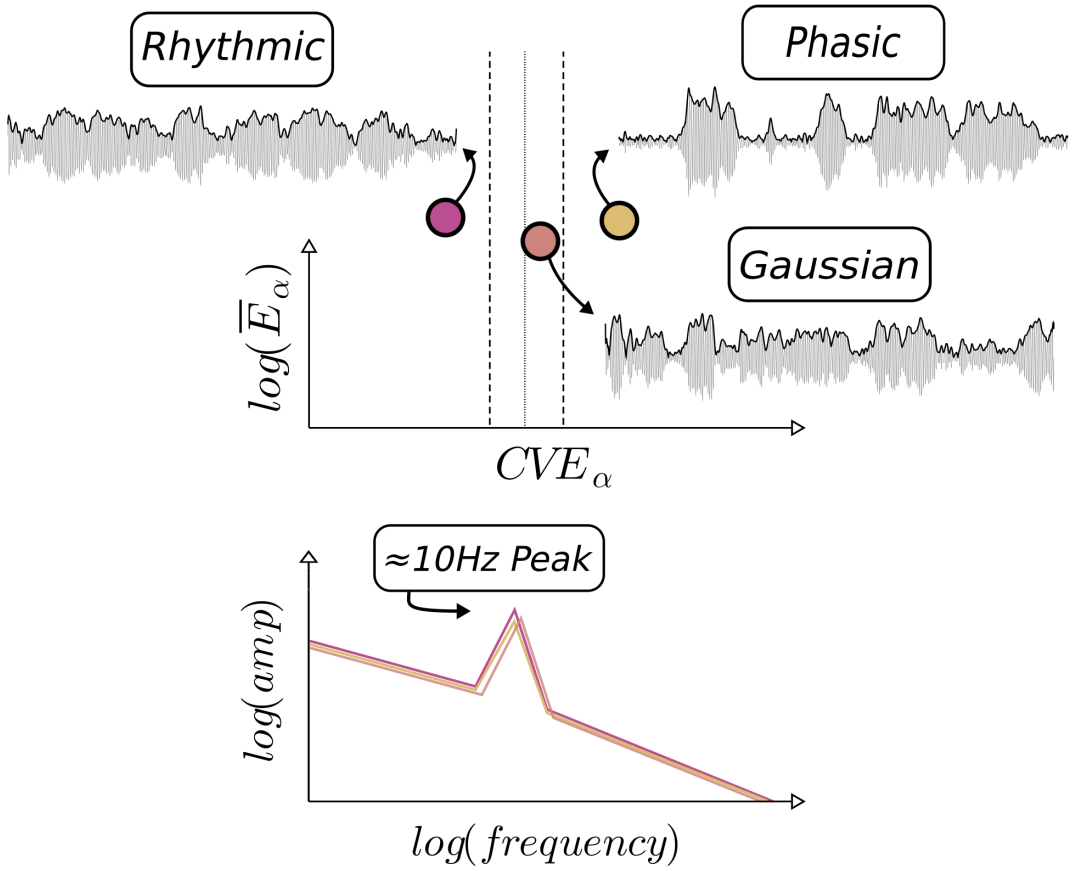

Figure 5.1: Summary of main results. The human alpha rhythm displays Gaussian and synchronous amplitude modulation patterns as revealed by the CVE. Gaussian, phasic, and rhythmic profiles — the three different dynamics detectable using CVE — were observed in alpha rhythm epochs, even though these same epochs showed very similar spectra, thus demonstrating that CVE captures signal information that is lost using spectral analysis alone.

BIBLIOGRAPHY

Acebrón, Juan A, Luis L Bonilla, Conrad J Pérez Vicente, Félix Ritort, and Renato Spigler (2005). "The Kuramoto model: A simple paradigm for synchronization phenomena". *Reviews of modern physics* 77.1, p. 137.

Adrian, Edgar Douglas and Brian HC Matthews (1934a). "The Berger rhythm: potential changes from the occipital lobes in man". *Brain* 57.4, pp. 355–385.

— (1934b). "The interpretation of potential waves in the cortex". *The Journal of Physiology* 81.4, p. 440.

Adrian, Edgar Douglas and Kazumi Yamagiwa (1935). "The origin of the Berger rhythm." *Brain: A Journal of Neurology*.

Association, World Medical et al. (2001). "World Medical Association Declaration of Helsinki. Ethical principles for medical research involving human subjects." *Bulletin of the World Health Organization* 79.4, p. 373.

Attal, Yohan, Burkhard Maess, Angela Friederici, and Olivier David (2012). "Head models and dynamic causal modeling of subcortical activity using magnetoencephalographic/electroencephalographic data". *Reviews in the Neurosciences* 23.1, pp. 85–95.

Avitan, Lilach, Mina Teicher, and Moshe Abeles (2009). "EEG generator—a model of potentials in a volume conductor". *Journal of neurophysiology* 102.5, pp. 3046–3059.

Babayan, Anahit, Miray Erbey, Deniz Kumral, Janis D Reinelt, Andrea MF Reiter, Josefin Röbbig, H Lina Schaare, Marie Uhlig, Alfred Anwander, Pierre-Louis Bazin, et al. (2019). "A mind-brain-body dataset of MRI, EEG, cognition, emotion, and peripheral physiology in young and old adults". *Scientific data* 6, p. 180308.

Barlow, John S (1985). "Methods of analysis of nonstationary EEGs, with emphasis on segmentation techniques: a comparative review." *Journal of clinical neurophysiology: official publication of the American Electroencephalographic Society* 2.3, pp. 267–304.

Berger, Hans (1929). "Über das elektroenkephalogramm des menschen". *Archiv für psychiatrie und nervenkrankheiten* 87.1, pp. 527–570.

Bezanson, Jeff, Alan Edelman, Stefan Karpinski, and Viral B Shah (2017). "Julia: A fresh approach to numerical computing". *SIAM review* 59.1, pp. 65–98.

Breakspear, Michael, Stewart Heitmann, and Andreas Daffertshofer (2010). "Generative models of cortical oscillations: neurobiological implications of the Kuramoto model". *Frontiers in human neuroscience* 4, p. 190.

Butcher, John Charles (1996). "A history of Runge-Kutta methods". *Applied numerical mathematics* 20.3, pp. 247–260.

Buzsáki, György (2006). *Rhythms of the Brain*. Oxford University Press.

Buzsáki, György, Costas Anastassiou, and Christof Koch (2012). "The origin of extracellular fields and currents—EEG, ECoG, LFP and spikes". *Nature reviews neuroscience* 13.6, p. 407.

Buzsáki, György, Nikos Logothetis, and Wolf Singer (2013). "Scaling brain size, keeping timing: evolutionary preservation of brain rhythms". *Neuron* 80.3, pp. 751–764.

Caton, Richard (1875). "The electric currents of the brain". *Br Med J* 2, p. 278.

Cohen, Leon (1995). *Time-frequency analysis*. Vol. 778. Prentice hall.

Cohen, Michael X (2017). "Where does EEG come from and what does it mean?" *Trends in neurosciences* 40.4, pp. 208–218.

Colombo, Michele Angelo, Martino Napolitani, Melanie Boly, Olivia Gosseries, Silvia Casarotto, Mario Rosanova, Jean-Francois Brichant, Pierre Boveroux, Steffen Rex, Steven Laureys, et al. (2019). "The spectral exponent of the resting EEG indexes the presence of consciousness during unresponsiveness induced by propofol, xenon, and ketamine". *Neuroimage* 189, pp. 631–644.

Cooper, Ray, AL Winter, HJ Crow, and W Grey Walter (1965). "Comparison of subcortical, cortical and scalp activity using chronically indwelling electrodes in man". *Electroencephalography and clinical neurophysiology* 18.3, pp. 217–228.

Corsini, Giovanni and Roberto Saletti (1988). "A 1/f/sup gamma/power spectrum noise sequence generator". *IEEE Transactions on Instrumentation and Measurement* 37.4, pp. 615–619.

Cramér, Harald (1970). *Random variables and probability distributions*. Tech. rep.

Crameri, Fabio (2018). "Scientific colour-maps". *Zenodo*. DOI: 10.5281/zenodo.1243862.

Cumin, David and CP Unsworth (2007). "Generalising the Kuramoto model for the study of neuronal synchronisation in the brain". *Physica D: Nonlinear Phenomena* 226.2, pp. 181–196.

Davis, Hallowell and Pauline A Davis (1936). "Action potentials of the brain: In normal persons and in normal states of cerebral activity". *Archives of Neurology & Psychiatry* 36.6, pp. 1214–1224.

Dehghani, Nima, Claude Bédard, Sydney S Cash, Eric Halgren, and Alain Destexhe (2010). "Comparative power spectral analysis of simultaneous elecroencephalographic and magnetoencephalographic recordings in humans suggests non-resistive extracellular media". *Journal of computational neuroscience* 29.3, pp. 405–421.

Dick, Donald E and Avery O Vaughn (1970). "Mathematical description and computer detection of alpha waves". *Mathematical Biosciences* 7.1-2, pp. 81–95.

Díaz, Javier, Alejandro Bassi, Alex Coolen, Ennio A Vivaldi, and Juan-Carlos Letelier (2018). "Envelope analysis links oscillatory and arrhythmic EEG activities to two types of neuronal synchronization". *Neuroimage* 172, pp. 575–585.

Díaz, Javier, Pablo Razeto-Barry, Juan-Carlos Letelier, John Caprio, and Juan Bacigalupo (2007). "Amplitude modulation patterns of local field potentials reveal asynchronous neuronal populations". *Journal of Neuroscience* 27.34, pp. 9238–9245.

Elul, Rafael (1969). "Gaussian behavior of the electroencephalogram: changes during performance of mental task". *Science* 164.3877, pp. 328–331.

— (1972). "The genesis of the EEG". In: *International review of neurobiology*. Vol. 15. Elsevier, pp. 227–272.

Folland, Gerald B and Alladi Sitaram (1997). "The uncertainty principle: a mathematical survey". *Journal of Fourier analysis and applications* 3.3, pp. 207–238.

Fonov, Vladimir, Alan C Evans, Kelly Botteron, C Robert Almli, Robert C McKinstry, D Louis Collins, Brain Development Cooperative Group, et al. (2011). "Unbiased average age-appropriate atlases for pediatric studies". *Neuroimage* 54.1, pp. 313–327.

Frauscher, Birgit, Nicolas Von Ellenrieder, Rina Zelmann, Irena Doležalová, Lorella Minotti, André Olivier, Jeffery Hall, Dominique Hoffmann, Dang Khoa Nguyen, Philippe Kahane, et al. (2018). "Atlas of the normal intracranial electroencephalogram: neurophysiological awake activity in different cortical areas". *Brain* 141.4, pp. 1130–1144.

Gabor, Dennis (1946). "Theory of communication. Part 1: The analysis of information". *Journal of the Institution of Electrical Engineers-Part III: Radio and Communication Engineering* 93.26, pp. 429–441.

Gebber, Gerard L, Sheng Zhong, Craig Lewis, and Susan M Barman (1999). "Human brain alpha rhythm: nonlinear oscillation or filtered noise?" *Brain research* 818.2, pp. 556–560.

Gibbs, Frederic Andrews, Hallowell Davis, and William G Lennox (1935). "The electro-encephalogram in epilepsy and in conditions of impaired consciousness". *Archives of Neurology & Psychiatry* 34.6, pp. 1133–1148.

Gloor, Pierre (1969). "Hans Berger on electroencephalography". *American Journal of EEG Technology* 9.1, pp. 1–8.

Gonen, Fahrettin F and Gleb V Tcheslavski (2012). "Techniques to assess stationarity and gaussianity of EEG: An overview". *International Journal of Bioautomation* 16.2, pp. 135–142.

Grant, Gunnar (2006). "The 1932 and 1944 Nobel Prizes in physiology or medicine: rewards for ground-breaking studies in neurophysiology". *Journal of the History of the Neurosciences* 15.4, pp. 341–357.

Grass, Albert M (1984). "The electroencephalographic heritage until 1960". *American Journal of EEG Technology* 24.3, pp. 133–173.

Grass, Albert M and Frederic A Gibbs (1938). "A Fourier transform of the electroencephalogram". *Journal of neurophysiology* 1.6, pp. 521–526.

Haken, Hermann (1996). *Principles of Brain Functioning*. Springer.

He, Biyu J (2014). "Scale-free brain activity: past, present, and future". *Trends in cognitive sciences* 18.9, pp. 480–487.

Hidalgo, Víctor Manuel, Javier Díaz, Jorge Mpodozis, and Juan-Carlos Letelier (2021). "Envelope analysis of the human alpha rhythm". *bioRxiv*.

Hodgkin, Alan (1979). "Edgar Douglas Adrian, Baron Adrian of Cambridge, 30 November 1889 - 4 August 1977". *Biographical Memoirs of Fellows of the Royal Society* 25, pp. 1–73.

Hutcheon, Bruce and Yosef Yarom (2000). "Resonance, oscillation and the intrinsic frequency preferences of neurons". *Trends in neurosciences* 23.5, pp. 216–222.

Izhikevich, Eugene M and Yoshiki Kuramoto (2006). "Weakly coupled oscillators". *Encyclopedia of mathematical physics* 5, p. 448.

Jasper, H and C Stefanis (1965). "Intracellular oscillatory rhythms in pyramidal tract neurones in the cat". *Electroencephalography and clinical neurophysiology* 18.6, pp. 541–553.

Jones, Stephanie R (2016). "When brain rhythms aren't 'rhythmic': implication for their mechanisms and meaning". *Current Opinion in Neurobiology* 40, pp. 72–80.

Kane, Nick, Jayant Acharya, Sandor Beniczky, Luis Caboclo, Simon Finnigan, Peter W Kaplan, Hiroshi Shibasaki, Ronit Pressler, and Michel JAM van Putten (2017). "A revised glossary of terms most commonly used by clinical electroencephalographers and updated proposal for the report format of the EEG findings. Revision 2017". *Clinical neurophysiology practice* 2, p. 170.

Khaluf, Yara, Eliseo Ferrante, Pieter Simoens, and Cristián Huepe (2017). "Scale invariance in natural and artificial collective systems: a review". *Journal of the royal society interface* 14.136, p. 20170662.

King, Frederick W (2009). *Hilbert transforms*. Vol. 1. Cambridge University Press Cambridge.

Klee, Maurice and Wilfrid Rall (1977). "Computed potentials of cortically arranged populations of neurons". *Journal of neurophysiology* 40.3, pp. 647–666.

Kormylo, J and V Jain (1974). "Two-pass recursive digital filter with zero phase shift". *IEEE Transactions on Acoustics, Speech, and Signal Processing* 22.5, pp. 384–387.

Kramer, Mark A, Adriano BL Tort, and Nancy J Kopell (2008). "Sharp edge artifacts and spurious coupling in EEG frequency comodulation measures". *Journal of neuroscience methods* 170.2, pp. 352–357.

Krishnaswamy, Pavitra, Gabriel Obregon-Henao, Jyrki Ahveninen, Sheraz Khan, Behtash Babadi, Juan Eugenio Iglesias, Matti S Hämäläinen, and Patrick L Purdon (2017). "Sparsity enables estimation of both subcortical and cortical activity from MEG and EEG". *Proceedings of the National Academy of Sciences* 114.48, E10465–E10474.

Ktonas, Periklis Y and Nicola Papp (1980). "Instantaneous envelope and phase extraction from real signals: theory, implementation, and an application to EEG analysis". *Signal Processing* 2.4, pp. 373–385.

Kuramoto, Yoshiki (1975). "Self-entrainment of a population of coupled non-linear oscillators". In: *International symposium on mathematical problems in theoretical physics*. Springer, pp. 420–422.

Kuramoto, Yoshiki and Ikuko Nishikawa (1987). "Statistical macrodynamics of large dynamical systems. Case of a phase transition in oscillator communities". *Journal of Statistical Physics* 49.3-4, pp. 569–605.

Lachaux, Jean-Philippe, Eugenio Rodriguez, Jacques Martinerie, and Francisco J Varela (1999). "Measuring phase synchrony in brain signals". *Human brain mapping* 8.4, pp. 194–208.

Lehmann, D (1971). "Multichannel topography of human alpha EEG fields". *Electroencephalography and clinical neurophysiology* 31.5, pp. 439–449.

Llinás, Rodolfo R (1988). "The intrinsic electrophysiological properties of mammalian neurons: insights into central nervous system function". *Science* 242.4886, pp. 1654–1664.

Loomis, Alered L, E Newton Harvey, and Garret Hobart (1935). "Potential rhythms of the cerebral cortex during sleep." *Science*.

Lopes da Silva, F.H. (1991). "Neural mechanisms underlying brain waves: from neural membranes to networks". *Electroencephalography and clinical neurophysiology* 79.2, pp. 81–93.

Lopes da Silva, F.H. and W Storm Van Leeuwen (1977). "The cortical source of the alpha rhythm". *Neuroscience letters* 6.2-3, pp. 237–241.

Lopes da Silva, F.H., THMT Van Lierop, CF Schrijer, and W Storm Van Leeuwen (1973). "Organization of thalamic and cortical alpha rhythms: spectra and coherences". *Electroencephalography and clinical neurophysiology* 35.6, pp. 627–639.

Lopes da Silva, F.H. and Ab van Rotterdam (2005). "Biophysical Aspects of EEG and Magnetoencephalogram Generation". In: *Electroencephalography: Basic principles, clinical applications, and related fields*. Ed. by Ernst Niedermeyer and Fernando Lopes da Silva. Lippincott Williams & Wilkins Philadelphia, pp. 107–126.

Lorente De Nó, Rafael (1947). "Action potential of the motoneurons of the hypoglossus nucleus". *Journal of cellular and comparative Physiology* 29.3, pp. 207–287.

Luo, Huageng, Xingjie Fang, and Bugra Ertas (2009). "Hilbert transform and its engineering applications". *AIAA journal* 47.4, pp. 923–932.

Marple, Lawrence (1999). "Computing the discrete-time" analytic" signal via FFT". *IEEE Transactions on signal processing* 47.9, pp. 2600–2603.

Matthews, Paul C, Renato E Mirollo, and Steven H Strogatz (1991). "Dynamics of a large system of coupled nonlinear oscillators". *Physica D: Nonlinear Phenomena* 52.2-3, pp. 293–331.

Matthews, Paul C and Steven H Strogatz (1990). "Phase diagram for the collective behavior of limit-cycle oscillators". *Physical review letters* 65.14, p. 1701.

Mazziotta, John, Arthur Toga, Alan Evans, Peter Fox, Jack Lancaster, Karl Zilles, Roger Woods, Tomas Paus, Gregory Simpson, Bruce Pike, et al. (2001). "A probabilistic atlas and reference system for the human brain: International Consortium for Brain Mapping (ICBM)". *Philosophical Transactions of the Royal Society of London. Series B: Biological Sciences* 356.1412, pp. 1293–1322.

McEwen, James A and Grant B Anderson (1975). "Modeling the stationarity and gaussianity of spontaneous electroencephalographic activity". *IEEE transactions on Biomedical Engineering* 5, pp. 361–369.

Millett, David (2001). "Hans Berger: From psychic energy to the EEG". *Perspectives in biology and medicine* 44.4, pp. 522–542.

Milotti, Edoardo (2002). "1/f noise: a pedagogical review". *arXiv: Classical Physics*.

Mimura, Keiichi (1971). "On the periodic fluctuations of alpha waves". *The Japanese journal of physiology* 21.4, pp. 375–386.

Mitra, Partha P and Bijan Pesaran (1999). "Analysis of dynamic brain imaging data". *Biophysical journal* 76.2, pp. 691–708.

Motokawa, K and T Mita (1942). "Das Wharscheinlichkeitsprinzip über die Gehirn elektrischen Erscheinugen des Menschen". *Jap. J. Med. Sci. III. Biophys* 8, pp. 63–77.

Motokawa, Koiti (1943). "Eine statistisch= mechanische Theorie über das Elektrenke= phalogramm". *The Tohoku Journal of Experimental Medicine* 45.3-4, pp. 278–296.

Niedermeyer, Ernst (2005a). "Historical Aspects". In: *Electroencephalography: Basic principles, clinical applications, and related fields*. Ed. by Ernst Niedermeyer and Fernando Lopes da Silva. Lippincott Williams & Wilkins Philadelphia, pp. 1–16.

— (2005b). "The normal EEG of the waking adult". In: *Electroencephalography: Basic principles, clinical applications, and related fields*. Ed. by Ernst Niedermeyer and Fernando Lopes da Silva. Lippincott Williams & Wilkins Philadelphia, pp. 155–164.

Niedermeyer, Ernst and Fernando Lopes da Silva (2005). *Electroencephalography: basic principles, clinical applications, and related fields*. Lippincott Williams & Wilkins.

Nunez, Paul L and Ramesh Srinivasan (2006). *Electric fields of the brain: the neurophysics of EEG*. Oxford University Press, USA.

Oostenveld, Robert and Peter Praamstra (2001). "The five percent electrode system for high-resolution EEG and ERP measurements". *Clinical neurophysiology* 112.4, pp. 713–719.

Papoulis, Athanasios and S Unnikrishna Pillai (2002). *Probability, random variables, and stochastic processes*. Tata McGraw-Hill Education.

Pfurtscheller, G and R Cooper (1975). "Frequency dependence of the transmission of the EEG from cortex to scalp". *Electroencephalography and clinical neurophysiology* 38.1, pp. 93–96.

Pfurtscheller, Gert and FH Lopes Lopes da Silva (1999). "Event-related EEG/MEG synchronization and desynchronization: basic principles". *Clinical neurophysiology* 110.11, pp. 1842–1857.

Prast, JW (1949). "An interpretation of certain EEG patterns as transient responses of a transmission system". *Electroencephalography and clinical neurophysiology* 1.1-4, p. 370.

Prerau, Michael J, Ritchie E Brown, Matt T Bianchi, Jeffrey M Ellenbogen, and Patrick L Purdon (2017). "Sleep neurophysiological dynamics through the lens of multitaper spectral analysis". *Physiology* 32.1, pp. 60–92.

Purpura, Dominick P and Harry Grundfest (1956). "Nature of dendritic potentials and synaptic mechanisms in cerebral cortex of cat". *Journal of neurophysiology* 19.6, pp. 573–595.

Rackauckas, Christopher and Qing Nie (2017). "Differentialequations. jl–a performant and feature-rich ecosystem for solving differential equations in julia". *Journal of Open Research Software* 5.1.

Rao, R and E Edwards (2008). "Faculty Opinions Recommendation of [Díaz J et al., J Neurosci 2007 27(34):9238-9245]". *Faculty Opinions*. DOI: 10.3410/f.1127024.584154.

Riera, Jorge J, Takeshi Ogawa, Takakuni Goto, Akira Sumiyoshi, Hiroi Nonaka, Alan Evans, Hiroyoshi Miyakawa, and Ryuta Kawashima (2012). "Pitfalls in the dipolar model for the neocortical EEG sources". *Journal of neurophysiology* 108.4, pp. 956–975.

Rudrauf, David, Abdel Douiri, Christopher Kovach, Jean-Philippe Lachaux, Diego Cosmelli, Mario Chavez, Claude Adam, Bernard Renault, Jacques Martinerie, and Michel Le Van Quyen (2006). "Frequency flows and the time-frequency dynamics of multivariate phase synchronization in brain signals". *Neuroimage* 31.1, pp. 209–227.

Saunders, Michael G (1963). "Amplitude probability density studies on alpha and alpha-like patterns". *Electroencephalography and clinical Neurophysiology* 15.5, pp. 761–767.

Saxena, Garima, Awadhesh Prasad, and Ram Ramaswamy (2012). "Amplitude death: The emergence of stationarity in coupled nonlinear systems". *Physics Reports* 521.5, pp. 205–228.

Schroeder, MJ and RE Barr (2000). "An alpha modulation index for electroencephalographic studies using complex demodulation". *Medical and Biological Engineering and Computing* 38.3, pp. 306–310.

Schultheiss, Nathan W, Astrid A Prinz, and Robert J Butera (2012). *Phase response curves in neuroscience*. Springer.

Schwartz, Mischa, William R Bennett, and Seymour Stein (1995). *Communication systems and techniques*. John Wiley & Sons.

Seeber, Martin, Lucia-Manuela Cantonas, Mauritius Hoevels, Thibaut Sesia, Veerle Visser-Vandewalle, and Christoph M Michel (2019). "Subcortical electrophysiological activity is detectable with high-density EEG source imaging". *Nature communications* 10.1, pp. 1–7.

Singer, Wolf (1999). "Neuronal synchrony: a versatile code for the definition of relations?" *Neuron* 24.1, pp. 49–65.

Steriade, Mircea, PLRR Gloor, Rodolfo R Llinas, F.H. Lopes da Silva, and M-M Mesulam (1990). "Basic mechanisms of cerebral rhythmic activities". *Electroencephalography and clinical neurophysiology* 76.6, pp. 481–508.

Steriade, Mircea, David A McCormick, and Terrence J Sejnowski (1993a). "Thalamocortical oscillations in the sleeping and aroused brain". *Science* 262.5134, pp. 679–685.

Steriade, Mircea, Angel Nunez, and Florin Amzica (1993b). "A novel slow (< 1 Hz) oscillation of neocortical neurons in vivo: depolarizing and hyperpolarizing components". *Journal of neuroscience* 13.8, pp. 3252–3265.

Steriade, Mircea, Angel Nuñez, and Florin Amzica (1993c). "Intracellular analysis of relations between the slow (< 1 Hz) neocortical oscillation and other sleep rhythms of the electroencephalogram". *Journal of Neuroscience* 13.8, pp. 3266–3283.

Strogatz, Steven H (1994). "Norbert Wiener's brain waves". In: *Frontiers in mathematical biology*. Springer, pp. 122–138.

— (2000). "From Kuramoto to Crawford: exploring the onset of synchronization in populations of coupled oscillators". *Physica D: Nonlinear Phenomena* 143.1-4, pp. 1–20.

— (2018). *Nonlinear dynamics and chaos with student solutions manual: With applications to physics, biology, chemistry, and engineering*. CRC press.

Tasaki, Kyoji (1971). "Koiti Motokawa (1903-1971)." *Vision research* 11.12, p. 1369.

Theiler, James, Stephen Eubank, André Longtin, Bryan Galdrikian, and J Doyne Farmer (1992). "Testing for nonlinearity in time series: the method of surrogate data". *Physica D: Nonlinear Phenomena* 58.1-4, pp. 77–94.

Toman, James (1941). "Flicker potentials and the alpha rhythm in man". *Journal of neurophysiology* 4.1, pp. 51–61.

Wiener, Norbert (1948). *Cybernetics or control and communication in the animal and the machine*. Technology Press.

Winfree, Arthur T (1967). "Biological rhythms and the behavior of populations of coupled oscillators". *Journal of theoretical biology* 16.1, pp. 15–42.

PUBLICATIONS

This thesis produced the following publications:

Víctor Manuel Hidalgo, Javier Díaz, Jorge Mpodozis, and Juan-Carlos Letelier (2021). "Envelope analysis of the human alpha rhythm". *bioRxiv*

FUNDING

This work was funded by Fondecyt 1170027 to Dr. Jorge Mpodozis.